EMBRY-RIDDLE
Aeronautical University™
SCHOLARLY COMMONS

Dissertations and Theses

2014

Robust and Adaptive Nonlinear Control of Limit Cycle Oscillations in UAVs Using Synthetic Jet Actuators

Natalie Ramos Pedroza

Follow this and additional works at: https://commons.erau.edu/edt

Part of the Aeronautical Vehicles Commons, and the Engineering Physics Commons

Robust and Adaptive Nonlinear Control of Limit Cycle Oscillations in UAVs Using Synthetic Jet Actuators

by

Natalie Ramos Pedroza

A Thesis Submitted to the Physical Sciences Department

in Partial Fulfillment of the Requirements

for the Degree of

MASTER OF SCIENCE

(Engineering Physics)

Embry-Riddle Aeronautical University

Daytona Beach, FL 32114

2014

Robust and Adaptive Nonlinear Control of Limit Cycle Oscillations in UAVs Using Synthetic Jet Actuators

By

Natalie Ramos Pedroza

This thesis was prepared under the direction of the candidate's thesis committee chair, Dr. William MacKunis, Department of Physical Sciences, and has been approved by the members of the thesis committee. It was submitted to the College of Arts and Sciences and was accepted in partial fulfillment of the requirements for the Degree of

Master of Science in Engineering Physics

Thesis Review Committee:
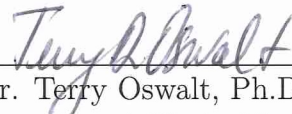
Dr. William MacKunis, Ph.D
Committee Chair

Dr. Sergey V. Drakunov, Ph.D
Committee Member
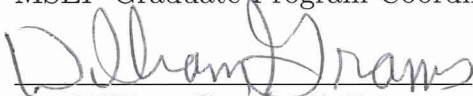
Dr. Vladimir Golubev, Ph.D
Committee Member
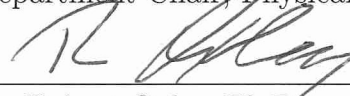
Dr. Peter Erdman, Ph.D
MSEP Graduate Program Coordinator

Dr. Terry Oswalt, Ph.D
Department Chair, Physical Sciences

Dr. William Grams, Ph.D
Dean, College of Arts & Sciences

Dr. Robert Oxley, Ph.D
Associate Vice President of Academics

11-21-14
Date

Acknowledgments

I would like to give thanks and gratitude to Dr. William MacKunis for his knowledge, patience, guidance, support, and dedication. I would like to give my gratitude to Sam because he was always there supporting me.

I would also like to thank my family, especially my brother and sister for being an inspiration to me.

Abstract

Limit cycle oscillations (LCO), also known as flutter, cause significant challenges in flight control of unmanned aerial vehicles (UAVs), and could potentially lead to structural damage and catastrophic failures. LCO can be described as vibrational motions in the pitching and plunging displacements of an aircraft wing. Even in low Reynolds number (low-Re) flight regimes, LCO can exceed the limiting boundary for safe UAV flight. Further, as practical considerations motivate the design of smaller, lighter weight UAVs, there is a growing need for UAV systems that do not require heavy mechanical actuators (e.g., ailerons). To address this, the use of synthetic jet actuators (SJAs) in UAV flight control systems is becoming popular as a practical alternative to mechanical deflection surfaces. SJAs are promising tools for LCO suppression systems in small UAVs due to their small size, ease of operation, and low cost. Uncertainties inherent in the dynamics of SJAs present significant challenges in SJA-based control design. Specifically, the input-output characteristic of SJAs is nonlinear and contains parametric uncertainty. Further control design challenges exist in situations where multiple actuators lose effectiveness. In the event of loss of effectiveness in multiple actuators, control challenges arise due to the fact that the resulting system contains fewer actuators than degrees of freedom (DOF) to be controlled (i.e., an underactuated system). Still further difficulties exist in control design for dual parallel underatuated systems, where standard backstepping-based control approaches cannot be applied. In this thesis, three nonlinear SJA-based control methods are presented, which are capable of complete (i.e., asymptotic) suppres-

sion of LCO in UAV systems containing uncertainty. An adaptive control method is presented first, which is shown to achieve asymptotic regulation of LCO for UAVs in the presence of model uncertainty and unmodelled external disturbances. Motivated by the desire to reduce the computational complexity of the closed-loop system, a structurally simplistic robust (single feedback loop) control design is presented next, which is shown to achieve asymptotic LCO regulation without the need for adaptive parameter estimation. Finally, to address the control challenges encountered in the event of actuator faults, a robust control method is presented, which achieves simultaneous suppression of the pitching and plunging displacements using only a single scalar control input. The control design presented for this underactuated scenario is also proven to completely compensate for the inherent SJA nonlinearity. Rigourous Lyapunov-based stability analyses are provided to prove the theoretical results, and numerical simulation results are provided to complement the theoretical development.

Contents

List of Tables

List of Figures

Chapter 1

Introduction

In this section, brief introductions to the concepts relevant to this thesis are presented. Specifically, this section will provide explanations related to LCO in aircaft wings, the engineering of SJA and philosophical motivation for their use in LCO suppression and aircraft tracking control applications, and summaries of the nonlinear control methods presented in this thesis.

LCO (Khalil, 2002; O'Donnell, Marzocca, & Milanese, 2007) result from nonlinearities (i.e nonlinear stiffness properties) inherent in the aeroelastic dynamics of a UAV system (Satak, Hernandez, & Hurtado, 2012). Suppression of LCO, or also known as flutter, is an important concern in UAV flight control applications.

Limit cycle oscillations are described as periodic motion of the pitching and plunging displacements in the UAV wing. Limit cycle oscillations can result when the state trajectories of a nonlinear ordinary differential equation exhibit stable periodic orbits in the neighborhood of an equilibrium point. Figure 1.1 shows where the location of the pitching and plunging motions would be in a standard airfoil (Beran, Pettit, &
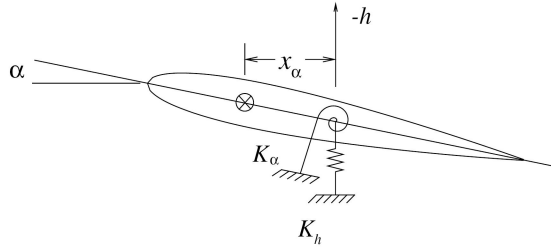
Figure 1.1: Illustration of pitch and plunge on an airfoil .

Millman, 2006). Due to these behaviors, the LCO could exceed the limiting safe flight boundaries of an aircraft (Rubillo, Bollt, & Marzocca, 2005) and could potentially lead to structural damages and catastrophes. Control applications for LCO suppression are often developed (Frampton & Clark, 2000; Strganac, K., & Thompson, 2000; Platanitis & Strganac, 2004) using mechanical deflection surfaces (e.g. flaps, ailerons, rudders, and elevators). To address this, the use of SJAs in UAV flight control systems is becoming popular as a practical alternative to mechanical deflection surfaces.

SJAs are promising tools for LCO suppression systems in UAVs due to their small size, ease of operation, and low cost. SJAs transfer linear momentum to a flow system by using a vibrating diaphragm, which creates trains of vortices through the alternating ejection and suction of fluid through a small orifice (see Figure 1.2. Since these vortices (i.e., jets) are formed entirely from the fluid (i.e., air) of the flow system, a key benefit of SJAs is that they achieve this transfer of momentum with zero net mass injection across the flow boundary. Thus, SJAs do not require space for a fuel supply. SJAs can be utilized to modify the boundary layer flow field near the surface of a UAV wing, and this capability can be applied to achieve LCO suppression for UAVs. Uncertainties inherent in the dynamics of SJAs present significant challenges in SJA-based control design, however. Specifically, the input-output characteristic of SJAs

is nonlinear and contains parametric uncertainty. Further control design challenges exist in situations where multiple actuators lose effectiveness. Such underactuated scenarios create significant control design challenges, since there are fewer control actuators than degrees of freedom to be controlled.

Over the last few years, several SJA-based nonlinear control methods have been presented, which utilize neural networks and/or complex fluid dynamics computations in the feedback loop (e.g., see (Tchieu, Kutay, Muse, Calise, & Leonard, 2008; Mondschein, Tao, & Burkholder, 2011; Deb, Tao, Burkholder, & Smith, 2005a, 2005b; Deb, Burkholder, & Smith, 2006; Deb, Tao, Burkholder, & Smith, 2007, 2008; Liu et al., 2006; Singhal, Tao, & Burkholder, 2009; Tao, 1996; Jee et al., 2009; Milanese, De Breuker, Marzocca, & Abdalla, 2008)). While these approaches have been shown to perform well in their respective control tasks, function approximation methods and complex calculations in the control loop can require increased computational resources, which might not be available in small UAV applications. Adaptive control approaches have been applied to linear time invariant (LTI) dynamic models to compensate for SJA nonlinearities and external disturbances (Mondschein et al., 2011). Adaptive inverse control schemes are another popularly utilized method to compensate for the actuator nonlinearity inherent in SJAs (Deb et al., 2005a, 2005b, 2006, 2007, 2008). Motivated by the desire to compensate for the SJA nonlinearity with a more simplified structure, a robust inverse control method is presented in (Mackunis et al., 2013), which is proven to achieve asymptotic SJA-based flight tracking without the use of adaptive update laws or function approximation.

Control design for underactuated systems presents further control challenges. While backstepping-based approaches can be utilized for underactuated system in a

cascade or normal form (Oland, Schlanbush, & Kristiansen, 2013; Yoshimura, Watanabe, & Maeyama, 2013; Gao et al., 2012), additional challenges exist for systems in a parallel underactuated form, where backstepping techniques cannot be applied. There remains a need for computationally minimal robust nonlinear control methods, which can achieve asymptotic regulation for dual parallel systems, where a single scalar control input simultaneously affects two states.
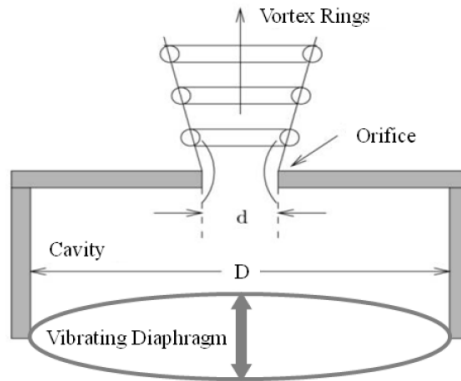
Figure 1.2: Schematic layout of a Synthetic Jet Actuator.

This thesis will investigate and compare different types of nonlinear control methods for LCO suppression, including robust control techniques and an adaptive control approach. In addition, a robust sliding mode control (SMC) design will be investigated, which compensates for SJA nonlinearities while achieving simultaneous pitching and plunging suppression using a single scalar control input, (i.e., a dual parallel system).

The chapters in this thesis are organized as follows: Chapter 2 introduces the relevant mathematical methods, including state space systems, stability definitions, Lyapunov's first and second stability theorems, nonlinear damping, adaptive control,

and sliding mode control. Chapter 3 deals with SJA-based LCO suppression using an adaptive control method. Chapter 4 presents a structurally simplistic robust (single feedback loop) control design. Chapter 5 extends the previous results by developing a robust control method to compensate for the SJA nonlinearity in a single input-two output system. Chapter 6 presents and summarizes the results and discusses directions for future work.

Chapter 2

Mathematical Methods

This chapter provides descriptions of the key mathematical methods used in this thesis. It includes definitions of Lyapunov's first and second stability theorems and details on the basic control design methods of nonlinear damping, adaptive control, and sliding mode control.

2.1 System Stability

In control engineering, stability properties are an important concept in understanding the characteristics of a dynamical system. An equilibrium point, x^*, is considered *stable* if all solutions starting at nearby points stay nearby. The equilibrium point would be *unstable* if it is not stable. An equilibrium point is *asymptotically stable* if all solutions starting in the vicinity of the equilibrium point converge to the equilibrium point as time approaches infinity.

2.2   Stability Definitions

Consider a dynamic system in the form

$$\dot{x} \;=\; f(x, t) \tag{2.1}$$

where

$$x = \begin{bmatrix} x_1 & x_2 & \ldots & x_n \end{bmatrix}^T. \tag{2.2}$$

In (2.2), $x(t)$ denotes the state vector, and $f : [0, \infty) \times \mathcal{D} \to \mathbb{R}^n$ is piecewise continuous in t and locally uniformly continuous in $x(t)$ on $\mathcal{D}$, where $\mathcal{D} \subset \mathbb{R}^n$ is a domain that contains the origin $x(t) = 0$. Without loss of generality, it will be assumed in the following discussion that the equilibrium point under consideration is at the origin $x(t) = 0$. This choice is arbitrary however, because a simple coordinate transformation can be utilized such that the equilibrium point could be any value of $x(t)$ on $\mathcal{D}$. Consider the isolated equilibrium point, $x^* = 0$, which satisfies

$$f(x^*, t) = 0 \quad \forall t \geq 0 \tag{2.3}$$

- The equilibrium point is *stable* if for every $\epsilon > 0$, there exists a positive, $\delta = \delta(\epsilon, t_0) > 0$ such that

$$\|x(t_0)\| < \delta \Rightarrow \|x(t)\| < \epsilon, \quad \forall t \geq t_0 \geq 0 \tag{2.4}$$

where $\| \cdot \|$ denotes the Euclidean norm of a vector, which is defined as

$$\|x\| \equiv \sqrt{x^T x}. \tag{2.5}$$

If, in addition, δ does not depend on t_0, then the equilibrium point is uniformly stable.

- The equilibrium point, x^*, is *locally asymptotically stable* (LAS) if is stable (2.4) and

$$\|x(t_0) - x^*\| < \delta \Rightarrow x(t) \to x^*, \quad t \to \infty \tag{2.6}$$

- The equilibrium point is *globally asymptotically stable* (GAS) if it is stable and

$$x(t) \to x^* \quad t \to \infty \quad \forall x(t_0). \tag{2.7}$$

- The equilibrium point is *unstable*, if it is not *stable*.

2.2.1 Stability Analysis for Linear and Nonlinear Systems

Consider a dynamic system in the form

$$\dot{x} = f(x, t) \tag{2.8}$$

where $x(t) \in \mathcal{D} \subset \mathbb{R}^n$, and $f : [0, \infty) \times \mathcal{D} \to \mathbb{R}^n$ is locally Lipschitz and piecewise continuous. A function $f : \mathbb{R} \times \mathbb{R} \to \mathbb{R}^n$ is considered *Lipschitz* (Khalil, 2002) if it

satisfies the inequality

$$\|f(x,t) - f(y,t)\| \leq L\|x - y\| \quad \forall(x,t) \quad \text{and} \quad \forall(y,t) \tag{2.9}$$

in some neighborhood of (x_0, t_0), where L is the positive Lipschitz constant. The domain $\mathcal{D}$ contains the origin. Using the following transformation

$$z = x - x^* \tag{2.10}$$

where $z(t)$ is a small perturbation from the equilibrium point, x^*, the following equation can be obtained:

$$\dot{x} = \dot{z} = f(x^* + z, t) \tag{2.11}$$

The expression in (2.11) can be linearized at x^* and expressed in the form

$$\dot{z} = Az \tag{2.12}$$

where A is the following constant Jacobian matrix evaluated at x^*

$$A \triangleq \frac{\partial f}{\partial x}|_{x^*}. \tag{2.13}$$

The origin of the linearized system (2.12), $z = 0$, is *asymptotically stable* if all the eigenvalues of the Jacobian matrix, A, have negative real parts. It is stable if the eigenvalues do not have any positive real parts and if there are no repeated eigenvalues on the imaginary axis.

2.2.2   Lyapunov Stability

In this thesis, *Lyapunov analyses* were used to determine the stability properties of the closed-loop systems. Lyapunov analysis is a well-accepted tool for determining the stability properties of nonlinear differential equations, without explicitly solving the equations.

2.2.2.1   Lyapunov's First Stability Theorem

Lyapunov's first stability theorem linearizes a nonlinear system near the equilibrium point, x^*, and can be utilized to analyze the local stability properties of the nonlinear system in the neighborhood of the equilibrium point.

- If the origin $z = 0$ of the linearized system is *asymptotically stable*, then the equilibrium point, x^* of the nonlinear system is *locally asymptotically stable*.

- If the origin $z = 0$ of the linearized system is *unstable*, then the equilibrium point, x^* of the nonlinear system is *unstable*.

- Nothing can be said about the equilibrium point, x^*, of the nonlinear system, if the origin $z = 0$ of the linearized system is *stable*.

2.2.2.2   Lyapunov's Second Stability Theorem

Lyapunov's second stability theorem uses a positive definite potential function, called a Lyapunov function, $V(x)$, which helps evaluate the stability of a nonlinear system without solving or linearizing the nonlinear system.

Consider a dynamic system in the following form

$$\dot{x} = f(x, t) \quad f(x^*, t) = 0 \tag{2.14}$$

where x^* is the equilibrium point of the system. In some finite region $\mathcal{D}$ containing x^*, assume there exists a positive definite continuously differentiable Lyapunov function $V : \mathcal{D} \to \mathbb{R}$.

- The equilibrium point is *stable* if

$$V(x) > 0 \quad \text{in} \quad \mathcal{D} - \{0\} \quad \text{and} \quad V(0) = 0 \quad \forall t \tag{2.15}$$

  and its time derivative along trajectories of the system is negative semi-definite in the sense that

$$\dot{V}(x) \leq 0 \tag{2.16}$$

- The equilibrium point is *locally asymptotically stable* if (2.15) is satisfied and $\dot{V}(x)$ is **negative definite** in the sense that

$$\dot{V}(x) < 0 \quad \text{in} \quad \mathcal{D} - \{0\} \quad \text{and} \quad \dot{V}(0) = 0 \quad \forall t \tag{2.17}$$

- The equilibrium point is *globally asymptotically stable*, if (2.15) is satisfied for any initial state $x(t_0)$, the time derivative of the Lyapunov candidate function is **negative definite**, and the function $V(x)$ is radially unbounded in the sense

11

that

$$\|x(t)\| \to \infty \Rightarrow V(x) \to \infty \tag{2.18}$$

- The equilibrium point is *unstable* if

$$\dot{V}(x) \;>\; 0 \quad \forall x \neq 0 \tag{2.19}$$

$$\dot{V}(0) \;=\; 0 \quad \forall t \tag{2.20}$$

2.3 Barbalat's lemma

In addition to basic stability definitions and methods for determining the stability properties of equilibrium points, there are some basic mathematical definitions that prove useful in analyzing the dynamic properties of dynamical systems. The following definition of uniform continuity is an important definition, which is utilized in the subsequently defined lemma. (Stewart, 2012)

Definition 1. *Let $\mathcal{S}$ be a subset of $\mathbb{R}$. A function $f : \mathcal{S} \to \mathbb{R}$ is uniformly continuous on $\mathcal{S}$ if, for each $\epsilon > 0$, there exists a real number $\delta > 0$ such that $|f(x) - f(y)| < \epsilon$ for all x, $y \in \mathcal{S}$ with $|x - y| < \delta$, where δ depends on ϵ.*

Lemma 1. *Barbalat's lemma (Khalil, 2002). Let $x : \mathbb{R} \to \mathbb{R}$ be a uniformly continuous function on $[0, \infty)$. Presume that the following exist and is finite*

$$\lim_{t \to \infty} \int_0^t x(\tau) d\tau \tag{2.21}$$

12

Then

$$x(t) \to 0 \quad as \quad t \to \infty \tag{2.22}$$

2.4 Nonlinear State Control

In this section, the robust and adaptive nonlinear state control methods used in this thesis are explained. In the robust control section, the methods of nonlinear damping and sliding mode control will both be described.

2.4.1 Adaptive Control

The *adaptive control method* provides a technique to stabilize a nonlinear system by using a time-varying control element to compensate for constant or slowly time-varying parametric uncertainty in the dynamic model (Landau, Lozano, M'Saad, & Karimi, 2011). Figure 2.1 illustrates a general adaptive control system. Consider a first-order nonlinear system described by the model

$$\dot{x} = f(x, t) + u, \tag{2.23}$$

where $x(t) \in \mathbb{R}^n$, and $u(t) \in \mathbb{R}^n$, and $f(x, t) \in \mathbb{R}^n$. Assume that the term $f(x, t)$ contains parametric uncertainty, which is linearly parameterizable in the sense that

$$f(x, t) = Y\theta, \tag{2.24}$$

13

where $Y(x) \in \mathbb{R}^{n \times p}$ denotes a measurable regression matrix, and $\theta \in \mathbb{R}^p$ is a vector containing the unknown constant system parameters. Thus, the dynamics can be rewritten as

$$\dot{x} = Y\theta + u \tag{2.25}$$

Since the elements of the vector θ are completely unknown, θ cannot be used in the feedback control law. In this case, the control law $u(t)$ can be designed using an estimate $\hat{\theta}(t)$ of the uncertain vector θ. The adaptive control law can then be designed as

$$u = -k_s x - Y\hat{\theta} \tag{2.26}$$

After substituting the control input $u(t)$, the closed-loop system can be expressed as

$$\dot{x} = Y\tilde{\theta} - k_s x \tag{2.27}$$

where $\tilde{\theta}(t) = \theta - \hat{\theta}(t)$ denotes the parameter estimate mismatch, and $k_s > 0$ is a positive constant control gain. The parameter estimate $\hat{\theta}$ is generated online using the adaptive update law

$$\dot{\hat{\theta}} = \text{proj}\left(Y^T x\right) \tag{2.28}$$

14
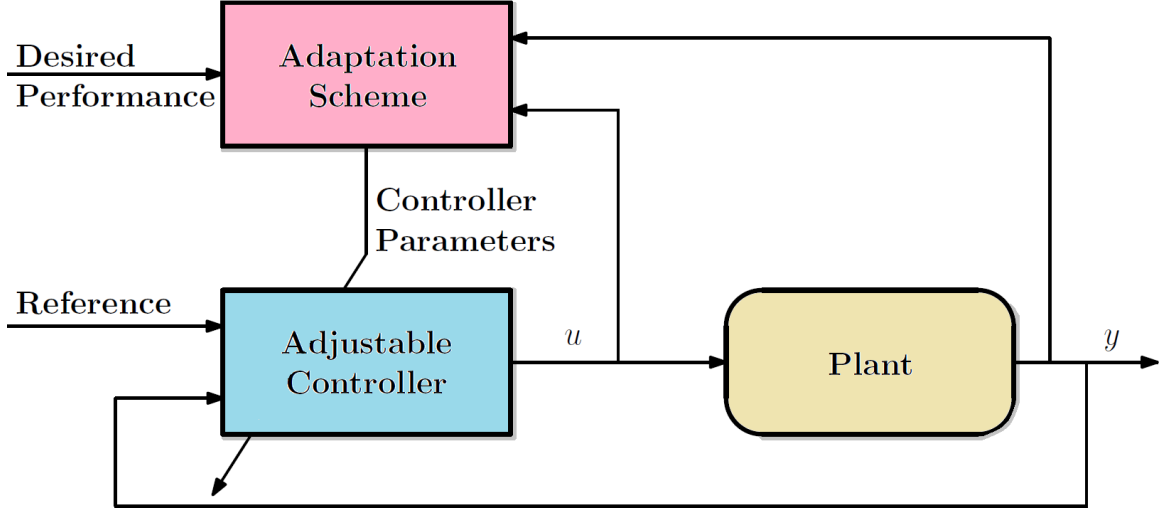
Figure 2.1: An adaptive control system

where $\text{proj}\,(\cdot)$ is a normal projection algorithm that ensures the following inequalities are satisfied (Dixon, 2007)

$$\underline{\theta} \;\leq\; \hat{\theta} \leq \bar{\theta} \tag{2.29}$$

where $\underline{\theta}$, $\bar{\theta}$ denote known lower and upper bounds on $\hat{\theta}\,(t)$.

To analyze the stability of the closed-loop system, consider the positive definite Lyapunov function

$$V\left(x,\tilde{\theta}\right) = \frac{1}{2}\tilde{\theta}^T\tilde{\theta} + \frac{1}{2}x^Tx. \tag{2.30}$$

After taking the time derivative of (2.30) and substituting (2.27), $\dot{V}(t)$ is obtained as

$$\dot{V} = x^T(Y\tilde{\theta} - k_s x) - \tilde{\theta}^T\dot{\hat{\theta}} \tag{2.31}$$

After substituting (2.28) into (2.31) the Lyapunov derivative can be found to satisfy

$$\dot{V}(t) = -k_s x^2 \leq 0 \tag{2.32}$$

Thus, since $\dot{V}(t)$ is negative semi-definite, the system is stable in the sense of Lyapunov. However, Since $\dot{V}(t) \leq 0$, $V(t)$ can never increase, so it remains bounded $\forall t$. Then, by integrating both sides of (2.32), the following is obtained

$$\int_0^t \dot{V}(\tau)d\tau \quad \leq \quad -k_s \int_0^t \|x(\tau)\|^2 d\tau \tag{2.33}$$

$$\int_0^t \|x(\tau)\|^2 d\tau \quad \leq \quad \frac{1}{k_s}\left(V(0) - V(t)\right) < \infty \tag{2.34}$$

By taking the limit of $t \to \infty$ and because $V(t)$ is a constant and/or decreasing from $V(0)$, the following equation is obtained

$$\lim_{t \to \infty} \int_0^t \|x(\tau)\|^2 d\tau \quad \leq \quad \lim_{t \to \infty} \frac{1}{k_s}\left(V(0) - V(t)\right) < \infty \tag{2.35}$$

Based on the assumption that $V(0) \in \mathcal{L}_\infty$, the inequalities (2.35) are used to prove that $x(t) \in \mathcal{L}_\infty \cap \mathcal{L}_2$. Since $x(t) \in \mathcal{L}_\infty$, the expression in (2.27) can be used to prove that $\dot{x}(t) \in \mathcal{L}_\infty$, thus $x(t)$ is uniformly continuous. Hence, Barbalat's lemma that is explained in Section 2.3 can now be used to prove that $\|x(t)\| \to 0$ as $t \to \infty$.

2.4.2 Robust Control

Using *robust control* methods, the effects of any uncertainty and disturbances in the nonlinear system are assumed to be bounded, and high-frequency or high-gain feedback is utilize to suppress or eliminate their detrimental effects. The following

sections describe the nonlinear damping and sliding mode control approaches for reducing these disturbances and stabilizing the closed-loop system.

2.4.2.1 Nonlinear Damping

In nonlinear control reducing the disturbance effects is important and helps to eliminate state-state error. By using the *nonlinear damping method*, these disturbances can be reduced to an arbitrarily small residual set (i.e., an ultimately bounded error). The resulting solution converges to a finite bounded set of the origin, which can be rendered arbitrarily small, but the tracking error cannot be driven to zero using nonlinear damping. Consider the scalar system

$$\dot{x} = f(x,t) + u(t) \tag{2.36}$$

where $x(t) \in \mathbb{R}^n$ is the state space vector, $u(t) \in \mathbb{R}^n$ is the control input vector, and $f(x,t) \in \mathbb{R}$ is an unknown disturbance that is bounded and sufficiently smooth in the sense that

$$|f(x,t)| \leq \zeta \quad |\dot{f}(x,t)| \leq \zeta_0 \tag{2.37}$$

where ζ, $\zeta_0 \in \mathbb{R}^+$ are known constants. A control design , $u(t)$, is incorporated to minimize $x(t)$ as

$$u = -(k_s + 1)x \tag{2.38}$$

17

where $k_s \in \mathbb{R}^+$ is the nonlinear damping gain (k_s could also be defined as a positive definite diagonal gain matrix). The closed loop dynamics are obtained when (2.38) is substituted into (2.36) as

$$\dot{x} = f(x,t) - (k_s + 1)x \tag{2.39}$$

To analyze the stability of (2.39), consider the following positive definite Lyapunov function and its derivative

$$V = \frac{1}{2}x^2 \tag{2.40}$$

$$\dot{V} = x\dot{x} \tag{2.41}$$

Substituting (2.39) into (2.41) results in

$$\dot{V} = xf(x,t) - (k_s + 1)x^2 \tag{2.42}$$

After completing the squares, the Lyapunov derivative can be expressed as

$$\dot{V} \leq -x^2 - k_s\left(|x|^2 - \frac{\zeta}{k_s}|x|\right) \tag{2.43}$$

$$\dot{V} \leq -x^2 + \frac{\zeta^2}{4k_s} \leq -2V + \frac{\zeta^2}{4k_s} \tag{2.44}$$

Based on the expression in (2.44), $x(t)$ is bounded and converges to the compact set described as

$$\mathcal{S} = \left\{x \mid |x| \leq \frac{\zeta}{2\sqrt{k_s}}\right\}. \tag{2.45}$$

18

Note that the size of the ultimate bound on the tracking error can be made arbitrarily small by increasing the control gain k_s.

2.4.2.2 Sliding Mode Control

A *sliding mode control method* (SMC) forces state trajectories to reach a sliding manifold in finite time and to remain on the manifold for all future time (Utkin, 1992). Standard SMC uses a discontinuous control signal that causes the state to asymptotically converge to the desired state or to the origin. Consider a second order system given by

$$\dot{x}_1 = x_2 \tag{2.46}$$

$$\dot{x}_2 = h(x) + g(x)u \tag{2.47}$$

where $h(x)$ and $g(x)$ are unknown nonlinear functions, and $g(x) \geq g_0 \geq 0$ for all x. By selecting the sliding manifold as

$$s = a_1 x_1 + x_2 = 0, \tag{2.48}$$

then $\dot{x}_1 = -a_1 x_1$, and the control gain $a_1 > 0$ can be selected to yield the desired rate of convergence of the state $x_1(t)$ to zero. The motion on the manifold $s = 0$ is independent of h and g. Taking the time derivative of (2.48) and using (2.46) and (2.47), $\dot{s}$ is obtained as

$$\dot{s} = a_1 \dot{x}_1 + \dot{x}_2 \tag{2.49}$$

$$\dot{s} = a_1 x_2 + h(x) + g(x)u \tag{2.50}$$

19

It is assumed that $h(x)$ and $g(x)$ satisfy the inequality

$$\left| \frac{a_1 x_2 + h(x)}{g(x)} \right| \leq \varrho(x), \quad \forall x \in \mathbb{R}^2 \tag{2.51}$$

for some known function $\varrho(x)$. Consider a positive definite Lyapunov candidate function, $V(x)$, as

$$V = \frac{1}{2} s^2 \tag{2.52}$$

After taking the time derivative of (2.52) and using (2.50) and (2.51), the following upper bound is obtained:

$$\dot{V} = s\dot{s} = s \left[a_1 x_2 + h(x) \right] + g(x)su \leq g(x)|s|\varrho(x) + g(x)su \tag{2.53}$$

A sliding mode control law can be designed as

$$u = -\beta(x)\text{sign}(s) \tag{2.54}$$

where $\beta(x) \geq \varrho(x) + \beta_0$, $\beta_0 > 0$, and where the sgn(s) denotes the discontinuous signum function, which is defined as

$$\text{sign}(s) = \begin{cases} 1 & s > 0 \\ 0 & s = 0 \\ -1 & s < 0 \end{cases} \tag{2.55}$$

Note that this is a simplification of the signum function, which is being used here to simplify the Lyapunov-based stability analysis. The signum function is actually defined such that the value at zero (i.e., the sgn(0)) is included in the set $(-1, +1)$ (Filippov, 1964). To analyze the stability properties of the system using the actual definition of the signum function, differential inclusions would be required, and this analysis is not included in this thesis.

The Lyapunov derivative can be expressed as

$$
\begin{aligned}
\dot{V} &= g(x)|s|\varrho(x) - g(x)\left[\varrho(x) + \beta_0\right] s\,\mathrm{sgn}(s) & (2.56) \\
&= -g(x)\beta_0|s| \leq -g_0\beta_0|s| & (2.57)
\end{aligned}
$$

It can be shown that $W = \sqrt{2V} = |s|$ satisfies the differential inequality

$$
D^+ W \leq g_0\beta_0 \tag{2.58}
$$

where D^+ denotes the upper right-hand derivative (also known as the Dini derivative)

Remark 1. *The upper Dini derivative of a continuous function $f : \mathbb{R} \to \mathbb{R}$ is denoted as f'_+ and is defined as*

$$
f'_+(t) \triangleq \lim_{h \to 0+} \sup \frac{f(t+h) - f(t)}{h}. \tag{2.59}
$$

The comparison lemma (Khalil, 2002) can then be used to show that

$$
W(s(t)) \leq W(s(0)) - g_0\beta_0 t \tag{2.60}
$$

This shows that the trajectory reaches the manifold $s(x) = 0$ in finite time, where it will remain. Thus, $x_1(t) \to 0$ as $t \to \infty$.

2.5 Summary of Mathematical Methods

This chapter described the different mathematical methods that are going to be used throughout this thesis to investigate methods to suppress LCO in a nonlinear system. These oscillations can be suppressed by using the different nonlinear control methods described in Section 2.4.1 and 2.4.2.

Chapter 3

LCO suppression using adaptive control

3.1 Introduction

In this chapter, a SJA-based nonlinear adaptive controller to suppress limit cycle oscillations is developed in systems with uncertain actuator dynamics. This work was published in IFAC 2014 World Conference with the title *Lyapunov-Based Adaptive Regulation of Limit Cycle Oscillations in Aircraft Wings Using Synthetic Jet Actuators* by (Ramos Pedroza, MacKunis, Guenthoer, Golubev, & Curtis, 2014).

A Lyapunov-based stability analysis was used to prove asymptotic plunging regulation which includes a detailed dynamic model for the pitching and plunging dynamics. Numerical simulation results are provided to demonstrate that simultaneous pitching and plunging suppression is achieved using the control law that only uses the plunging terms.

3.2 Dynamic Model

The equation describing limit cycle oscillations in an airfoil approximated as a 2-dimensional thin plate can be expressed as

$$M_s\ddot{p} + C_s\dot{p} + F(p)p = \begin{bmatrix} -\text{Lift} \\ \text{Moment} \end{bmatrix} \tag{3.1}$$

where the coefficients M_s, $C_s \in \mathbb{R}^{2\times2}$ denote the structural mass and damping matrices, $F(p) \in \mathbb{R}^{2\times2}$ is a nonlinear stiffness matrix, and $p(t) \in \mathbb{R}^2$ denotes the state vector. In (3.1), $p(t)$ is explicitly defined as

$$p = \begin{bmatrix} h \\ \alpha \end{bmatrix} \tag{3.2}$$

where $h(t)$, $\alpha(t) \in \mathbb{R}$ denote the plunging [*meters*] and pitching [*radians*] displacements describing the LCO effects. Also in (3.1), the structural linear mass matrix M_s is defined as (Theodorsen, 1935)

$$M_s = \begin{bmatrix} m & S_\alpha \\ S_\alpha & I_\alpha \end{bmatrix} \tag{3.3}$$

where the parameters S_α, $I_\alpha \in \mathbb{R}$ are the static moment and moment of inertia in [$kg \cdot m$], respectively. The structural linear damping matrix is described as

$$C_s = 2\begin{bmatrix} \zeta_h\sqrt{k_h m} & 0 \\ 0 & \zeta_a\sqrt{k_\alpha I_\alpha} \end{bmatrix} \tag{3.4}$$

where the parameters ζ_h, $\zeta_\alpha \in \mathbb{R}$ are the damping logarithmic decrements for plunging and pitching, and $m \in \mathbb{R}$ is the mass of the wing in $[kg]$, or in this case, a flat plate. The nonlinear stiffness matrix utilized in this study is

$$F(p) = \begin{bmatrix} k_h & 0 \\ 0 & k_\alpha + k_{\alpha^3}\alpha^2 \end{bmatrix} \tag{3.5}$$

where k_α, $k_{\alpha^3} \in \mathbb{R}$ denote structural resistances to pitching (linear and nonlinear) in $[\frac{N}{m}]$ and $k_h \in \mathbb{R}$ is the structural resistance to plunging in $[\frac{N}{m}]$. The right hand side of (3.1) is given by (Theodorsen, 1935)

$$\begin{aligned} \begin{bmatrix} -\text{Lift} \\ \text{Moment} \end{bmatrix} &= \begin{bmatrix} -(L + L_{v_j}) \\ (M + M_{v_j}) \end{bmatrix} \\ &= M_a\ddot{p} + C_a\dot{p} + K_a p + L_\eta\eta + B_1 v_j + B_2\dot{v}_j \end{aligned} \tag{3.6}$$

where $L_{v_j}(t)$, $M_{v_j}(t) \in \mathbb{R}$ denote the control contributions due to the SJA, and L, $M \in \mathbb{R}$ are the aerodynamic lift and moment due to the 2 degrees-of-freedom motions (Milanese et al., 2008). The $\eta \in \mathbb{R}^2$ are the aerodynamic state vectors that relates the moment and lift to the modes. Terms $v_j(t) \in \mathbb{R}$ and $\dot{v}_j(t) \in \mathbb{R}$ are the SJA control input (air) velocity in $[\frac{m}{s}]$ and acceleration in $[\frac{m}{s^2}]$, respectively. The constant vectors

B_1, $B_2 \in \mathbb{R}^{2\times 2}$ are defined

$$B_1 = \begin{bmatrix} -U\rho b I_1 \\ U\rho b^2 I_2 + aU\rho b^2 I_1 \end{bmatrix} \tag{3.7}$$

$$B_2 = \begin{bmatrix} -\rho b^2 I_2 \\ -\dfrac{1}{2}\rho b^3 I_3 + a\rho b^3 I_2 \end{bmatrix} \tag{3.8}$$

where the constant $\rho \in \mathbb{R}$ denotes the density of air in $[\frac{kg}{m^3}]$, and $U \in \mathbb{R}$ is the mean free-stream velocity in $[\frac{m}{s}]$. The parameters a, $b \in \mathbb{R}$ denote the relative location of the rotational axis from the midchord and the semi-chord in $[m]$, respectively. The functions I_1, I_2, $I_3 \in \mathbb{R}$ (Milanese et al., 2008) are linked to the control force distribution, and they are explicitly defined as

$$I_1 = \int_{\Theta_1}^{\Theta_2} \sin(\Theta)\tan^{-1}\left(\frac{\Theta}{2}\right) d\Theta \tag{3.9}$$

$$I_2 = \frac{1}{2}\left[\Theta_2 - \Theta_1 + \frac{1}{2}\sin(2\Theta_1) - \frac{1}{2}\sin(2\Theta_2)\right] \tag{3.10}$$

$$I_3 = \frac{1}{3}\left[\sin^3(\Theta_2) - \sin^3(\Theta_1)\right]. \tag{3.11}$$

The parameters Θ_1 and Θ_2 are the optimal synthetic jet locations (Milanese et al., 2008). The aerodynamic matrices M_a, C_a, $K_a \in \mathbb{R}^{2\times 2}$ and the aerodynamic state

matrix $L_\eta \in \mathbb{R}^{2\times2}$ are described as

$$M_a = \pi\rho b^2 \begin{bmatrix} -1 & ba \\ ba & -b^2\left(\frac{1}{8} - a^2\right) \end{bmatrix} \tag{3.12}$$

$$C_a = \pi\rho b^2 \begin{bmatrix} 0 & -U \\ 0 & -Ub\left(\frac{1}{2} - a\right) \end{bmatrix} \tag{3.13}$$

$$+ 2\pi\rho Ub\phi(0) \begin{bmatrix} -1 & -b\left(\frac{1}{2} - a\right) \\ b\left(\frac{1}{2} + a\right) & b^2\left(\frac{1}{2} + a\right)\left(\frac{1}{2} - a\right) \end{bmatrix}$$

$$K_a = 2\pi\rho Ub\phi(0) \begin{bmatrix} 0 & -U \\ 0 & b\left(\frac{1}{2} + a\right)U \end{bmatrix} \tag{3.14}$$

$$L_\eta = 2\pi\rho Ub \begin{bmatrix} a_1 b_1 & a_2 b_2 \\ -b\left(\frac{1}{2} + a\right)a_1 b_1 & -b\left(\frac{1}{2} + a\right)a_2 b_2 \end{bmatrix} \tag{3.15}$$

where $\phi(0)$ is the Wagner solution function at 0, and the parameters a_1, b_1, a_2, $b_2 \in \mathbb{R}$ are the Wagner coefficients.

The aerodynamic state variables are governed by (Theodorsen, 1935)

$$\dot{\eta} = C_\eta \dot{p} + K_\eta p + S_\eta \eta \tag{3.16}$$

The aerodynamic state matrices in (3.16), C_η, K_η, $S_a \in \mathbb{R}^{2\times2}$, are explicitly defined

as

$$C_\eta = \frac{U}{b} \begin{bmatrix} -1 & -b\left(\frac{1}{2} - a\right) \\ -1 & -b\left(\frac{1}{2} - a\right) \end{bmatrix} \tag{3.17}$$

$$K_\eta = \frac{U}{b} \begin{bmatrix} 0 & -U \\ 0 & -U \end{bmatrix} \tag{3.18}$$

$$S_\eta = \frac{U}{b} \begin{bmatrix} -b_1 & 0 \\ 0 & -b_2 \end{bmatrix}. \tag{3.19}$$

By rearranging (3.1) and (3.6) and solving for $\ddot{p}(t)$, the equation becomes

$$\ddot{p} = -\frac{C}{M}\dot{p} - \frac{K}{M}p + \frac{L_\eta}{M}\eta + \frac{B_1}{M}v_j + \frac{B_2}{M}\dot{v}_j \tag{3.20}$$

where $C = C_s - C_a$, $K = F(p) - K_a$, and $M = M_s - M_a$.

The dynamic equation in (3.20) can be expressed in state form as

$$\dot{x} = A(x)x + \hat{B}_1 v_j + \hat{B}_2 \dot{v}_j \tag{3.21}$$

where $\dot{v}_j(t)$ denotes the control input, $x(t) \in \mathbb{R}^6$ is the state vector, $A(x) \in \mathbb{R}^{6 \times 6}$ is

the state matrix (nonlinear), and $\hat{B}_1$, $\hat{B}_2 \in \mathbb{R}^{6 \times 1}$ are defined as

$$
\hat{B}_1 = \begin{bmatrix} 0 \\ 0 \\ M^{-1}B_1 \\ 0 \\ 0 \end{bmatrix} \tag{3.22}
$$

$$
\hat{B}_2 = \begin{bmatrix} 0 \\ 0 \\ M^{-1}B_2 \\ 0 \\ 0 \end{bmatrix} \tag{3.23}
$$

where B_1 and B_2 are the control input gain terms, which only directly affect $\ddot{h}(t)$ and $\ddot{\alpha}(t)$. By making the definitions $x_1 = h$, $x_2 = \alpha$, $x_3 = \dot{h}$, $x_4 = \dot{\alpha}$, $x_5 = \eta_1$, and $x_6 = \eta_2$; and defining $\dot{x}_1 = x_3$, $\dot{x}_2 = x_4$, $\dot{x}_3 = \ddot{h}$, $\dot{x}_4 = \ddot{\alpha}$, $\dot{x}_5 = \dot{\eta}_1$, and $\dot{x}_6 = \dot{\eta}_2$, the state vector and its derivative can be expressed as

$$
x \triangleq \begin{bmatrix} x_1 & x_2 & x_3 & x_4 & x_5 & x_6 \end{bmatrix}^T, \tag{3.24}
$$

$$
\dot{x} \triangleq \begin{bmatrix} \dot{x}_1 & \dot{x}_2 & \dot{x}_3 & \dot{x}_4 & \dot{x}_5 & \dot{x}_6 \end{bmatrix}^T. \tag{3.25}
$$

After expressing (3.20) in state space form similar to (3.21) and solving for the corresponding coefficients, the $A(x)$ state matrix can be explicitly obtained.

3.3 Control Development

The objective is to design the scalar control signal $\dot{v}_j(t)$ to regulate the plunge dynamics (i.e., $h(t)$) to zero. The plunging dynamics can be expressed as

$$\begin{aligned} \ddot{h} &= -c_1\dot{h} - c_2\dot{\alpha} - c_3h - c_4\alpha + c_5\eta_1 + c_6\eta_1 \\ &+ b_1v_j + b_2\dot{v}_j \ , \end{aligned} \tag{3.26}$$

where c_1, c_2, c_3, c_4, c_5, $c_6 \in \mathbb{R}$ are the coefficients related to $A(x)$. The coefficients b_1 and b_2 are unknown constant control input gain terms, which relate the SJA dynamics to the plunging dynamics. The expression in (3.27) can be rewritten as

$$\ddot{h} = g(h, \alpha, \eta) + b_1v_j + b_2\dot{v}_j \tag{3.27}$$

where $g(h, \alpha, \eta)$ satisfies inequality

$$\|g(h, \alpha, \eta)\| \leq \rho_0\|z\|$$

where $\rho_0 \in \mathbb{R}^+$ is a known bounding constant, and $z(t) \in \mathbb{R}^{2n}$ is defined as

$$z \triangleq \begin{bmatrix} e & r \end{bmatrix}^T. \tag{3.28}$$

To facilitate the subsequent control development and stability analysis, a tracking error $e(t)$ and an auxiliary tracking error variable $r(t)$ are defined as

$$e = h - h_d = h - 0 \tag{3.29}$$

$$r = \dot{e} + \alpha_g e = \dot{h} + \alpha_g h \tag{3.30}$$

where $\alpha_g > 0 \in \mathbb{R}$ is a user defined control gain, and the desired plunging state $h_d = 0$ for the plunging suppression objective. To facilitate the following analysis, the time derivative of (3.30) is calculated as

$$\dot{r} = \ddot{h} + \alpha_g \dot{h}. \tag{3.31}$$

After substituting for $\ddot{h}(t)$ in (3.27) and using (3.31) the following is obtained:

$$\ddot{h} = g(h, \alpha, \eta) + Y_1 \theta_1 + \Omega \dot{v}_j$$

$$\dot{r} = g(h, \alpha, \eta) + Y_1 \theta_1 + \Omega \dot{v}_j + \alpha_g \dot{h} \tag{3.32}$$

where $Y_1(v_j) \in \mathbb{R}$ is measurable regressor, and $\theta_1 \in \mathbb{R}$ is an unknown constant defined via the parameterization

$$Y_1 \theta_1 \triangleq b_1 v_j.$$

In (3.32), $\Omega(b_2) \in \mathbb{R}$ denotes an uncertain constant auxiliary term defined via the parameterization

$$\Omega \dot{v}_j \triangleq b_2 \dot{v}_j. \tag{3.33}$$

The expression in (3.33) can be reparameterized in terms of a known regressor $Y_2(\dot{v}_j) \in \mathbb{R}$ and an unknown constant $\theta_2 \in \mathbb{R}$ as

$$\Omega \dot{v}_j \triangleq Y_2 \theta_2. \tag{3.34}$$

To address the issue of the control input $\dot{v}_j(t)$ being multiplied by the uncertain term Ω as in (3.32), an estimate of the uncertainty $\hat{\Omega}(t) \in \mathbb{R}$ is defined via

$$\hat{\Omega} \dot{v}_j \triangleq Y_2 \hat{\theta}_2 \tag{3.35}$$

where $\hat{\theta}_2(t) \in \mathbb{R}$ is a subsequently designed estimate of the parametric uncertainty in $\Omega(b_2)$. Based on (3.34) and (3.35), (3.32) can be expressed as

$$\dot{r} = g(h, \alpha, \eta) + \alpha_g \dot{h} + Y_1 \theta_1 + \hat{\Omega} \dot{v}_j + Y_2 \tilde{\theta}_2 \tag{3.36}$$

where the parameter estimate mismatch $\tilde{\theta}_2(t) \in \mathbb{R}$ is defined as

$$\tilde{\theta}_2 \triangleq \theta_2 - \hat{\theta}_2.$$

Based on the open-loop error dynamics in (3.36), the control input is designed as

$$\dot{v}_j = \hat{\Omega}^{-1} \left(-(k_s + 1) r - Y_1 \hat{\theta}_1 - h \right) \tag{3.37}$$

Remark 2. *Since the control input expression in (3.37) includes the internal dynamics of the SJA (i.e., since $\dot{v}_j$ depends on v_j), it is assumed in the subsequent analysis that the internal actuator dynamics are stable. The subsequent numerical simulation*

results show that this is a mild assumption.

Using (3.37) and the open loop dynamics in (3.36), the closed loop system would be

$$\dot{r} = \tilde{N} + Y_1\tilde{\theta}_1 + Y_2\tilde{\theta}_2 - (k_s + 1)\, r - h\ , \tag{3.38}$$

where the parameter estimate mismatch $\tilde{\theta}_1(t) \in \mathbb{R}$ is defined as

$$\tilde{\theta}_1 \triangleq \theta_1 - \hat{\theta}_1.$$

In (3.38), the unknown, unmeasurable auxiliary function $\tilde{N}(t) \in \mathbb{R}$ is defined as

$$\tilde{N} \triangleq g(h, \alpha, \eta) + \alpha_g \dot{h}.$$

The auxiliary term $\tilde{N}(t)$ satisfies the inequality

$$\|\tilde{N}\| \le \rho_z\|z\|.$$

where $\rho_z \in \mathbb{R}^+$ is a known bounding constant. Based on (3.38) and the following stability analysis, the adaptive estimates $\hat{\theta}_1(t)$ and $\hat{\theta}_2(t)$ are generated online according to the following adaptive update laws:

$$\dot{\hat{\theta}}_1 = \gamma_1\mathrm{proj}\left(Y_1^T r\right), \qquad \dot{\hat{\theta}}_2 = -\gamma_2\mathrm{proj}\left(Y_2^T r\right) \tag{3.39}$$

where γ_1, $\gamma_2 \in \mathbb{R}$ are positive constant adaptation gains.

3.4 Stability Analysis

Theorem 1. *The adaptive controller in (3.37) ensures asymptotic regulation of the plunging displacement in the sense that*

$$|h(t)| \to 0 \quad as \quad t \to \infty. \tag{3.40}$$

Proof. Let $V\left(r, h, \tilde{\theta}_1, \tilde{\theta}_2\right)$ denote the following radially unbounded positive definite Lyapunov function:

$$V = \frac{1}{2}h^2 + \frac{1}{2}r^2 + \frac{\gamma_1^{-1}}{2}\tilde{\theta}_1^2 + \frac{\gamma_2^{-1}}{2}\tilde{\theta}_2^2. \tag{3.41}$$

After taking the time derivative (3.41) and substituting (3.38) and (3.30), $\dot{V}(t)$ is obtained as

$$\begin{aligned}
\dot{V} &= r\left(Y_1\tilde{\theta}_1 + Y_2\tilde{\theta}_2 - (k_s + 1)r - h + \tilde{N}\right) \\
&+ h(r - \alpha_g h) - \gamma_1^{-1}\tilde{\theta}_1\dot{\hat{\theta}}_1 - \gamma_2^{-1}\tilde{\theta}_2\dot{\hat{\theta}}_2.
\end{aligned} \tag{3.42}$$

After using the adaptive laws in (3.39), the expression in (3.42) can be used to upper bound $V(t)$ as

$$\dot{V} \leq -\alpha_g\|h\|^2 + \left[\rho_z\|r\|\|z\| - k_s\|r\|^2\right] \tag{3.43}$$

After completing the squares for the bracketed term in (3.43), the upper bound on $\dot{V}(t)$ can be expressed as

$$\dot{V} \leq -\lambda\|z\|^2 + \frac{\rho_z^2\|z\|^2}{4k_s} \tag{3.44}$$

where $\lambda \triangleq \min\{\alpha_g, 1\}$ and $z(t)$ is defined in (4.27). The expressions in (3.41) and (3.44) can be used to conclude that $h(t) \in \mathcal{L}_\infty$ and $r(t) \in \mathcal{L}_\infty$. Since, $h(t), r(t) \in \mathcal{L}_\infty$,

34

$\dot{h}(t) \in \mathcal{L}_\infty$ from (3.30). Since $h(t)$, $r(t)$, $\tilde{\theta}_1(t)$, $\dot{\tilde{\theta}}_1(t) \in \mathcal{L}_\infty$, (3.38) can be used to prove that $\dot{r} \in \mathcal{L}_\infty$. Given that $\dot{h}(t)$, $\dot{r}(t) \in \mathcal{L}_\infty$, $z(t)$ is uniformly continuous. Based on the assumption of $V(0) \in \mathcal{L}_\infty$, the expressions in (3.44) and (3.41) can be used to prove that $z(t) \in \mathcal{L}_\infty \cap \mathcal{L}_2$. Barbalat's lemma explained in detail in Section 2.3 can now be utilized to prove that $\|z(t)\| \to 0$ as $t \to \infty$. Thus, based on the definition of $z(t)$, $\|h(t)\| \to 0$ as $t \to \infty$. Further, given that $V(t)$ in (3.41) is radially unbounded, convergence of $h(t)$ is guaranteed, regardless of initial conditions which signifies a global result. □

3.5 Simulation Results

A numerical simulation was created to demonstrate the performance of the control law developed in (3.37). The simulation is based on the dynamic model given in (3.1) and (3.16). The dynamic parameters utilized in the simulation are summarized in Table 3.2 and were obtained from (Golubev, Dreyer, Hollenshade, & Visbal, 2009).

Table 3.1: Manually selected gains for adaptive control

$\alpha_g = 2.5$	$\gamma_1 = 1$
$k_s = 1$	

The parameters $\Theta_1 = 1.6$ and $\Theta_2 = 1.7$ are the synthetic jet locations that result in a lift overshoot reduction of 21% (Milanese et al., 2008). These values are used in conjunction with the parameters I_1, I_2, and I_3 as described in (3.7) and (3.8). The control gains α_g, γ_1 and k_s were manually selected and described in Table 3.1.

Fig. 3.1 shows the time evolution of $h(t)$, which demonstrates the rapid conver-

gence of the system plunge to zero. Furthermore, Fig. 3.1 also shows that the pitching displacement $\alpha(t)$ also converges to zero quickly, as well as the control effort, $\dot{v}_j(t)$, used during closed-loop controller operation. The commanded control input remains within reasonable limits throughout the duration of the simulation.

Table 3.2: Constant parameters for adaptive control

$\rho = 1.225 \frac{kg}{m^3}$	$a = -0.24$	$U = 18 \frac{m}{s}$
$m = 2.55 kg$	$b = 0.11 m$	$v = 18 \frac{m}{s}$
$S_\alpha = 10.4 \times 10^{-3} kg \cdot m$	$a_1 = 0.1650$	$a_2 = 0.0455$
$I_\alpha = 2.51 \times 10^{-3} kg \cdot m$	$b_1 = 0.3350$	$b_2 = 0.3000$
$k_h = 450 \frac{N}{m}$	$k_\alpha = 9.3 \frac{N}{m}$	$k_{\alpha^3} = 55 \frac{N}{m}$
$\zeta_h = 5.5 \times 10^{-3}$	$\zeta_\alpha = 1.8 \times 10^{-2}$	
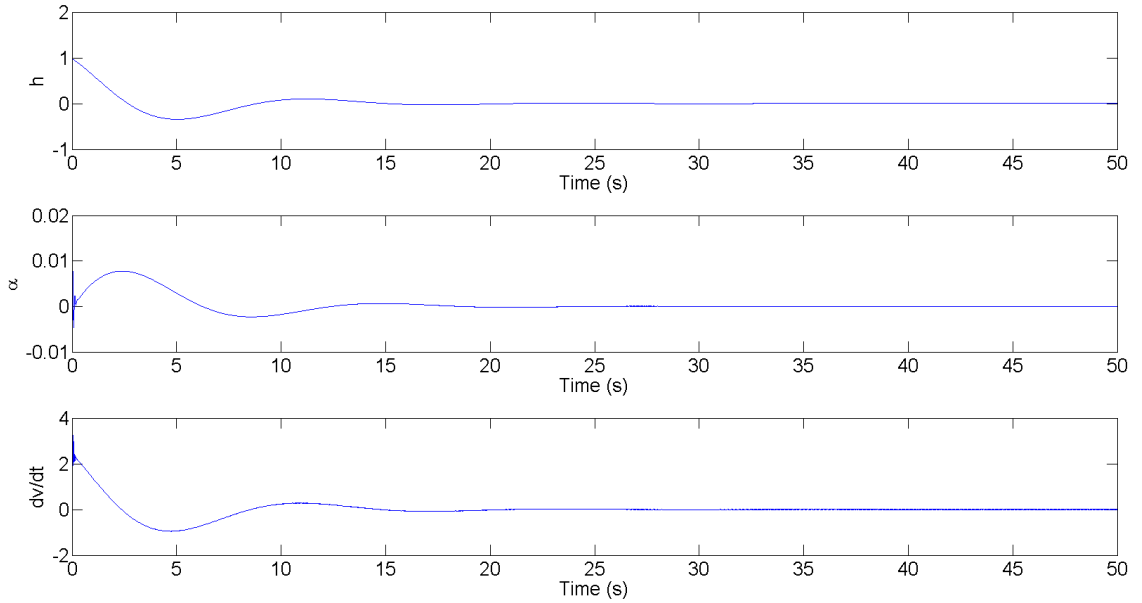
Figure 3.1: Convergence of the tracking error for plunging, h in $[m]$, pitching, α in $[rad]$, and control input behavior, $\dot{v}_j$ in $[\frac{m}{s^2}]$.

3.6 Conclusion

In this chapter, a nonlinear adaptive control law for LCO suppression was presented. The proposed control is proven to achieve global asymptotic regulation of the plunging displacement to zero in the presence of dynamic model uncertainties and uncertain actuator dynamics. Using numerical simulations, the control law described on Section 3.3 is also shown to suppress the pitching displacement $\alpha(t)$ to zero.

Chapter 4

LCO suppression using RISE

4.1 Introduction

In this chapter, a nonlinear robust controller is demonstrated to suppress limit cycle oscillations in a wing with an uncertain input control matrix. A Lyapunov-based stability analysis was used to proved local asymptotic regulation. Numerical simulation results are provided to demonstrate pitching and plunging suppression by using a sliding mode control law.

4.2 Dynamic Model

The equation describing LCO in an airfoil approximated as a 2-dimensional thin plate can be expressed as

$$M_s \ddot{p} + C_s \dot{p} + F(p)p = \begin{bmatrix} -Lift \\ Moment \end{bmatrix} \tag{4.1}$$

where the coefficients M_s, $C_s \in \mathbb{R}^{2\times 2}$ denote the structural mass and damping matrices, $F(p) \in \mathbb{R}^{2\times 2}$ is a nonlinear stiffness matrix, and $p(t) \in \mathbb{R}^2$ denotes the state vector. In (4.1), $p(t)$ is explicitly defined as

$$p = \begin{bmatrix} h \\ \alpha \end{bmatrix} \tag{4.2}$$

where $h(t)$, $\alpha(t) \in \mathbb{R}$ denote the plunging [meters] and pitching [radians] displacements describing the LCO effects. Also in (4.1), the structural linear mass matrix M_s (Theodorsen, 1935)

$$M_s = \begin{bmatrix} m & S_\alpha \\ S_\alpha & I_\alpha \end{bmatrix} \tag{4.3}$$

where the parameters S_α, $I_\alpha \in \mathbb{R}$ are the static moment and moment of inertia $[kg{\cdot}m]$, respectively. The structural linear damping matrix is described as

$$C_s = 2 \begin{bmatrix} \zeta_h \sqrt{k_h m} & 0 \\ 0 & \zeta_a \sqrt{k_\alpha I_\alpha} \end{bmatrix} \tag{4.4}$$

where the parameters ζ_h, $\zeta_\alpha \in \mathbb{R}$ are the damping logarithmic decrements for plunging and pitching, and $m \in \mathbb{R}$ is the mass of the wing in $[kg]$. The nonlinear stiffness matrix utilized in this study is

$$F(p) = \begin{bmatrix} k_h & 0 \\ 0 & k_\alpha + k_{\alpha^3}\alpha^2 \end{bmatrix} \tag{4.5}$$

where k_α, $k_{\alpha^3} \in \mathbb{R}$ denote structural resistances to pitching (linear and nonlinear) and $k_h \in \mathbb{R}$ is the structural resistance to plunging in $[\frac{N}{m}]$.

In (4.1), the total lift and moment are explicitly defined as

$$\begin{bmatrix} -Lift \\ Moment \end{bmatrix} = \begin{bmatrix} -(L + L_{v_j}) \\ (M + M_{v_j}) \end{bmatrix}$$

$$= M_a\ddot{p} + C_a\dot{p} + K_a p + L_\eta\eta + Bu$$

(4.6)

where $L_{vj}(t)$, $M_{vj}(t) \in \mathbb{R}$ denote the equivalent control force and moment generated by the jth SJA, and $L(t)$, $M(t) \in \mathbb{R}$ are the aerodynamic lift and moment due to the 2 degree-of-freedom motion (Milanese et al., 2008). In (4.6), $\eta(t) \in \mathbb{R}^2$ denotes the aerodynamic state vector that relates the moment and lift to the structural modes. Also in (4.6), $u(t) \in \mathbb{R}^2$ denotes the SJA-based control input (e.g., the SJA air velocity or acceleration), and $B \in \mathbb{R}^{2\times2}$ is an uncertain constant input gain matrix that relates the control input $u(t)$ to the equivalent force and moment generated by the SJA. Also in (4.6), the aerodynamic and mode matrices M_a, C_a, K_a, $L_\eta \in \mathbb{R}^{2\times2}$ are described as

$$M_a = \pi\rho b^2 \begin{bmatrix} -1 & ba \\ ba & -b^2\left(\frac{1}{8} + a^2\right) \end{bmatrix} \tag{4.7}$$

$$C_a = \pi\rho b^2 \begin{bmatrix} 0 & -U \\ 0 & -Ub\left(\frac{1}{2} - a\right) \end{bmatrix}$$

$$+ 2\pi\rho U b \phi(0) \begin{bmatrix} -1 & -b\left(\frac{1}{2} - a\right) \\ b\left(\frac{1}{2} + a\right) & b^2\left(\frac{1}{2} + a\right)\left(\frac{1}{2} - a\right) \end{bmatrix} \tag{4.8}$$

$$K_a = 2\pi\rho U b \phi(0) \begin{bmatrix} 0 & -U \\ 0 & b\left(\frac{1}{2} + a\right)U \end{bmatrix} \tag{4.9}$$

$$L_\eta = 2\pi\rho U b \begin{bmatrix} a_1 b_1 & a_2 b_2 \\ -b\left(\frac{1}{2} + a\right)a_1 b_1 & -b\left(\frac{1}{2} + a\right)a_2 b_2 \end{bmatrix} \tag{4.10}$$

where $\phi(0)$ is the Wagner solution function at 0, and the parameters a_1, b_1, a_2, $b_2 \in \mathbb{R}$ are the Wagner coefficients. The constant $\rho \in \mathbb{R}$ denotes the density of air in $\left[\frac{kg}{m^3}\right]$, and $U \in \mathbb{R}$ is the mean free-stream velocity in $\left[\frac{m}{s}\right]$. In addition, $a, b \in \mathbb{R}$ denote the relative locations of the rotational axis from the mid-chord and the semi-chord in $[m]$, respectively. The aerodynamic state variables are governed by (Theodorsen, 1935)

$$\dot{\eta} = C_\eta \dot{p} + K_\eta p + S_\eta \eta \tag{4.11}$$

The aerodynamic state matrices in (4.11), C_η, K_η, $S_\eta \in \mathbb{R}^{2\times 2}$, are explicitly defined

as

$$C_\eta = \frac{U}{b} \begin{bmatrix} -1 & -b\left(\dfrac{1}{2} - a\right) \\ -1 & -b\left(\dfrac{1}{2} - a\right) \end{bmatrix} \tag{4.12}$$

$$K_\eta = \frac{U}{b} \begin{bmatrix} 0 & -U \\ 0 & -U \end{bmatrix} \tag{4.13}$$

$$S_\eta = \frac{U}{b} \begin{bmatrix} -b_1 & 0 \\ 0 & -b_2 \end{bmatrix}. \tag{4.14}$$

By substituting (3.6) into (3.1), the LCO dynamics can be expressed as

$$\ddot{p} = -M^{-1}C\dot{p} - M^{-1}Kp + M^{-1}L_\eta\eta + M^{-1}Bu \tag{4.15}$$

where $C = C_s - C_a$, $K = F(p) - K_a$, and $M = M_s - M_a$. By making the definitions $x_1(t) = h(t)$, $x_2(t) = \alpha(t)$, $x_3(t) = \dot{h}(t)$, $x_4(t) = \dot{\alpha}(t)$, $x_5(t) = \eta_1(t)$, and $x_6(t) = \eta_2(t)$, the dynamic equation in (4.15) can be expressed in state form as

$$\dot{x} = A(x)x + \bar{B}u \tag{4.16}$$

where $x(t) \in \mathbb{R}^6$ is the state vector, $A(x) \in \mathbb{R}^{6\times6}$ is the state matrix (state-dependent). In (4.16), the input gain matrix $\bar{B} \in \mathbb{R}^{6\times2}$ is defined as

$$\bar{B} = \begin{bmatrix} 0_{2\times2} \\ M^{-1}B \\ 0_{2\times2} \end{bmatrix} \tag{4.17}$$

where $0_{2\times2}$ denotes a 2×2 matrix of zeros. The structure of the input gain matrix in (4.17) results from the fact that the control input $u(t)$ only directly affects $\ddot{h}(t)$ and $\ddot{\alpha}(t)$.

4.3 Control Development

The objective is to design the control signal $u(t)$ to regulate the plunge and pitching dynamics (*i.e.*, $h(t)$, $\alpha(t)$) to zero. To facilitate the control design, the expression in (4.15) is rewritten as

$$M\ddot{p} = g(h,\alpha,\eta) + Bu \tag{4.18}$$

where $g(h,\alpha,\eta)$ is an unknown, unmeasurable auxiliary function.

Remark 3. *Based on the open-loop error dynamics in (4.18), one of the control design challenges is that the control input $u(t)$ is premultiplied by the uncertain matrix B. In the following control development and stability analysis, it will be assumed that the matrix B is uncertain, and the robust control law will be designed with a constant feedforward estimate of the uncertain matrix. The simulation results demonstrate the capability of the robust control law to compensate for the input matrix uncertainty without the need for online parameter estimation or function approximators.*

To quantify the control objective, a regulation error $e_1(t) \in \mathbb{R}^2$ and auxiliary tracking error variables $e_2(t)$, $r(t) \in \mathbb{R}^2$ are defined as

$$e_1 = p - p_d \tag{4.19}$$

$$e_2 = \dot{e}_1 + \alpha_1 e_1 \tag{4.20}$$

$$r = \dot{e}_2 + \alpha_2 e_2 \tag{4.21}$$

where $\alpha_1, \alpha_2 > 0 \in \mathbb{R}^+$ are user-defined control gains, and the desired plunging and pitching states $p_d = [h, a]^T = [0, 0]^T$ for the plunging and pitching suppression objective. To facilitate the following analysis, (4.21) is premultiplied by M and the time derivative is calculated as

$$M\dot{r} = M\ddot{e}_2 + \alpha_2 M\dot{e}_2 \tag{4.22}$$

After using (4.18)–(4.21), the open-loop error dynamics are obtained as

$$M\dot{r} = \tilde{N} + N_d + B\dot{u} - e_2 \tag{4.23}$$

where the unknown, unmeasurable auxiliary functions $\tilde{N}(e_1, e_2, r)$, $N_d(p_d, \dddot{p}_d) \in \mathbb{R}^2$ are defined as

$$
\begin{aligned}
\tilde{N} &\triangleq \dot{g}(p, \eta) - \dot{g}(p_d, \eta) + \alpha_1 \left(r - \alpha_2 e_2 - \alpha_1 e_2 + \alpha_1^2 e_1 \right) \\
&\quad + \alpha_2 M \left(r - \alpha_2 e_2 \right) + e_2
\end{aligned}
\tag{4.24}
$$

$$N_d \triangleq -\dddot{p}_d + \dot{g}(p_d, \eta) \tag{4.25}$$

The motivation for defining the auxiliary functions in (4.24) and (4.25) is based on the fact that the following inequalities can be developed:

$$\|\tilde{N}\| \le \rho_0 \|z\|, \quad \|N_d\| \le \zeta_{N_d}, \quad \|\dot{N}_d\| \le \zeta_{\dot{N}_d} \tag{4.26}$$

where ρ_0, ζ_{N_d}, $\zeta_{\dot{N}_d} \in \mathbb{R}^+$ are known bounding constants, and $z(t) \in \mathbb{R}^6$ is defined as

$$z \triangleq \begin{bmatrix} e_1^T & e_2^T & r^T \end{bmatrix}^T \tag{4.27}$$

Based on the open-loop error dynamics in (4.23), the control input is designed via

$$\dot{u} = \hat{B}^{-1}(-(k_s + I_{2\times2})r - \beta sgn(e_2(t))) \tag{4.28}$$

where k_s, $\beta \in \mathbb{R}^{2\times2}$ denote constant, positive definite, diagonal control gain matrices, and $I_{2\times2}$ denotes a 2×2 identity matrix. In (4.28), $\hat{B} \in \mathbb{R}^{2\times2}$ denotes a constant, feedforward "best guess" estimate of the uncertain input gain matrix B. Note that the control input $u(t)$ does not depend on the unmeasurable acceleration term $r(t)$, since (4.28) can be directly integrated to show that $u(t)$ requires measurements of $e_1(t)$ and $e_2(t)$ only.

To facilitate the following stability proof, the control gain matrix β in (4.28) is selected to satisfy the sufficient condition

$$\lambda_{\min}(\beta) > \zeta_{N_d} + \frac{1}{\alpha_2}\zeta_{\dot{N}_d} \tag{4.29}$$

where $\lambda_{\min}(\cdot)$ denotes the minimum eigenvalue of the argument. After substituting (4.28) into (4.23), the closed-loop error dynamics are obtained as

$$M\dot{r} = \tilde{N} + N_d - (k_s + I_{n\times n})r + \beta sgn(e_2(t)) - e_2 \tag{4.30}$$

To reduce the complexity of the following stability analysis, it is assumed that the

product $B\hat{B}^{-1}$ is equal to identity. It can be proven that asymptotic regulation can be achieved for the case where the feedforward estimate $\hat{B}$ is within some prescribed finite range of the actual matrix B. The proof including the uncertainty in B is lengthy and is omitted here for brevity. The complete proof can be found in (MacKunis, Wilcox, Kaiser, & Dixon, 2010, 2009). The following simulation results demonstrate the performance of the controller in the presence of uncertainty in the input gain matrix B.

4.3.1   Stability Analysis

Theorem 2. *The controller given in (4.28) ensures asymptotic regulation of pitching and plunging displacements in the sense that*

$$\|e_1(t)\| \to 0 \qquad as \qquad t \to \infty \tag{4.31}$$

provided the control gain k_s is selected sufficiently large, and β is selected according to the sufficient condition in (4.29).

Lemma 2. *To facilitate the following proof, let $\mathcal{D} \subset \mathbb{R}^7$ be a domain containing $w(t) = 0$, where $w(t) \in \mathbb{R}^7$ is defined as*

$$w(t) \triangleq \begin{bmatrix} z^T & \sqrt{P(t)} \end{bmatrix}^T \tag{4.32}$$

In (4.32), the auxiliary function $P(t) \in \mathbb{R}$ is the generalized solution to the differential

equation

$$\dot{P}(t) = -L(t) \tag{4.33}$$

$$P(0) = \beta \left\| e_2(0) \right\| - N_d^T(0) e_2(0) \tag{4.34}$$

where the auxiliary function $L(t) \in \mathbb{R}$ is defined as

$$L(t) = r^T \left(N_d(t) - \beta sgn(e_2) \right) \tag{4.35}$$

Provided the sufficient condition in (4.29) is satisfied, the following inequality can be obtained:

$$\int_0^t L(\tau) d\tau \leq \beta \left\| e_2(0) \right\| - N_d^T(0) e_2(0) \tag{4.36}$$

Hence, (4.36) can be used to conclude that $P(t) \geq 0$.

Proof. Let $V(w,t) : \mathcal{D} \times [0, \infty) \to \mathbb{R}$ be defined as the nonnegative function

$$V(w,t) \triangleq \frac{1}{2} e_1^T e_1 + \frac{1}{2} e_2^T e_2 + \frac{1}{2} r^T M r + P \tag{4.37}$$

where $e_1(t)$, $e_2(t)$, and $r(t)$ are defined in (4.19)–(4.21), respectively; and the positive definite function $P(t)$ is defined in (4.33). The function $V(w,t)$ satisfies the inequality

$$U_1(w) \leq V(w,t) \leq U_2(w) \tag{4.38}$$

provided the sufficient condition introduced in (4.29) is satisfied, where $U_1(w)$, $U_2(w) \in$

$\mathbb{R}$ denote the positive definite functions

$$U_1 \triangleq \lambda_1 \|w\|^2, \qquad U_2 \triangleq \lambda_2 \|w\|^2 \tag{4.39}$$

where $\lambda_1 = \min\left\{\frac{1}{2}, \lambda_{\min}(M)\right\}$ and $\lambda_2 = \max\{1, \lambda_{\max}(M)\}$. After taking the time derivative of (4.37) and utilizing (4.20), (4.21), (4.30), and (4.33), $\dot{V}(w, t)$ can be upper bounded as

$$\dot{V}(w, t) \leq -\left(\alpha_1 - \frac{1}{2}\right)\|e_1\|^2 - \left(\alpha_2 - \frac{1}{2}\right)\|e_2\|^2 - \|r\|^2$$
$$-k_s \|r\|^2 + \rho_0 \|z\| \|r\| \tag{4.40}$$

where the bounds in (4.26) were used, and the fact that $e_1^T e_2 \leq \frac{1}{2}\|e_1\|^2 + \frac{1}{2}\|e_2\|^2$ (i.e., Young's inequality) was utilized. After completing the squares in (4.40), the upper bound on $\dot{V}(w, t)$ can be expressed as

$$\dot{V}(w, t) \leq -\left(\alpha_1 - \frac{1}{2}\right)\|e_1\|^2 - \left(\alpha_2 - \frac{1}{2}\right)\|e_2\|^2 - \|r\|^2$$
$$-k_s \left(\|r\| - \frac{\rho_0}{2k_s}\|z\|\right)^2 + \frac{\rho_0^2}{4k_s}\|z\|^2 \tag{4.41}$$

Since $k_s > 0$, the upper bound in (4.41) can be expressed as

$$\dot{V}(w, t) \leq -\left(\lambda_0 - \frac{\rho_0^2}{4k_s}\right)\|z\|^2 \tag{4.42}$$

where $\lambda_0 \triangleq \min\left\{\alpha_1 - \frac{1}{2}, \alpha_2 - \frac{1}{2}, 1\right\}$.

The following expression can be obtained from (4.42):

$$\dot{V}(w,t) \leq -U(w) \qquad (4.43)$$

where $U(w) = c\,\|z\|^2$, for some positive constant $c \in \mathbb{R}$, is a continuous, positive semi-definite function.

It follows directly from the Lyapunov analysis that $e_1(t)$, $e_2(t)$, $r(t) \in \mathcal{L}_\infty$. This implies that $\dot{e}_1(t)$, $\dot{e}_2(t) \in \mathcal{L}_\infty$ from the definitions given in (4.20) and (4.21). Given that $\dot{e}_1(t)$, $e_2(t)$, $r(t) \in \mathcal{L}_\infty$, it follows that $\ddot{e}_1(t) \in \mathcal{L}_\infty$ from (4.21). Thus, (4.19) can be used to prove that $p(t)$, $\dot{p}(t)$, $\ddot{p}(t) \in \mathcal{L}_\infty$. Since $p(t)$, $\dot{p}(t)$, $\ddot{p}(t) \in \mathcal{L}_\infty$, (4.18) can be used to prove that $u(t) \in \mathcal{L}_\infty$. Since $r(t)$, $u(t) \in \mathcal{L}_\infty$, (4.28) can be used to show that $\dot{u}(t) \in \mathcal{L}_\infty$. Given that $e_1(t)$, $e_2(t)$, $r(t)$, $\dot{u}(t) \in \mathcal{L}_\infty$, (4.30) can be used along with (4.26) to prove that $\dot{r}(t) \in \mathcal{L}_\infty$. Since $\dot{e}_1(t)$, $\dot{e}_2(t)$, $\dot{r}(t) \in \mathcal{L}_\infty$, $e_1(t)$, $e_2(t)$, $r(t)$, are uniformly continuous. In (4.27) can then be used to show that $z(t)$ is uniformly continuous. Given that $e_1(t)$, $e_2(t)$, $r(t) \in \mathcal{L}_\infty$, (4.37) and (4.42) can be used to prove that $z(t) \in \mathcal{L}_\infty \cap \mathcal{L}_2$. Barbalat's lemma explained in Section 2.3 can now be invoked to prove that $\|z(t)\| \to 0$ as $t \to \infty$. Hence, $\|e_1(t)\| \to 0$ as $t \to \infty$ from (4.27). Further, given that $V(w,t)$ in (4.37) is radially unbounded, convergence of $e_1(t)$ is guaranteed, regardless of initial conditions–a global results. $\qquad \square$

4.4   Results

A numerical simulation was created to demonstrate the performance of the control law developed in (4.28). In order to develop a realistic stepping stone to high-fidelity numerical simulation results using detailed computational fluid dynamics models, the

Table 4.1: Constant parameters for RISE control

$\rho = 1.225 \frac{kg}{m^3}$	$a = -0.24$	$U = 18.0 \frac{m}{s}$
$m = 2.55 kg$	$b = 0.11 m$	$v = 18 \frac{m}{s}$
$S_\alpha = 10.4 \times 10^{-3} kg \cdot m$	$a_1 = 0.1650$	$a_2 = 0.0455$
$I_\alpha = 2.51 \times 10^{-3} kg \cdot m$	$b_1 = 0.3350$	$b_2 = 0.3000$
$k_h = 450 \frac{N}{m}$	$k_\alpha = 9.3 \frac{N}{m}$	$k_{\alpha^3} = 55 \frac{N}{m}$
$\zeta_h = 5.5 \times 10^{-3}$	$\zeta_\alpha = 1.8 \times 10^{-2}$	

following simulation results are based on detailed dynamic parameters and specifications. The simulation is based on the dynamic model given in (4.1) and (4.11). The dynamic parameters utilized in the simulation are summarized in Table 4.1 and were obtained from (Golubev et al., 2009). The following simulation results were achieved using control gains defined as

$$\beta = \begin{bmatrix} 0.001 & 0 \\ 0 & 25 \end{bmatrix}, k_s = \begin{bmatrix} 0.00001 & 0 \\ 0 & 0.11 \end{bmatrix} \tag{4.44}$$

$$\alpha_1 = \begin{bmatrix} 1 & 0 \\ 0 & 35 \end{bmatrix}, \alpha_2 = \begin{bmatrix} 1 & 0 \\ 0 & 35 \end{bmatrix} \tag{4.45}$$

The control gains given in (4.44) and (4.45) were selected based on achieving a desirable response in terms of settling time and required control effort. To test the case where the input gain matrix B is uncertain, it is assumed in the simulation that the actual value of B is the 2×2 identity matrix, but the constant feedforward estimate

$\hat{B}$ used in the control law is given by

$$\hat{B} = \begin{bmatrix} 0.9 & 0.1 \\ -0.1 & 1.1 \end{bmatrix} \tag{4.46}$$

Fig. 4.1 shows the time evolution of $h(t)$, which demonstrates the rapid convergence of the system plunge to zero. Furthermore, Fig. 4.1 also shows that the pitching displacement $\alpha(t)$ also converges to zero quickly. In, Fig. 4.2, shows the convergence of the derivative for plunging, $\dot{h}$, and pitching, $\dot{\alpha}$. Fig. 4.3 shows the control effort force and moment used during closed-loop controller operation. Again, the commanded control input remains within reasonable limits throughout the duration of the simulation.

4.5   Conclusion

In this chapter, a nonlinear robust control law for synthetic jet based LCO suppression in UAV wings is presented. The robust control law in Section 4.3 achieves global asymptotic regulation of the pitching and plunging displacements to zero, $(h, \alpha) \to 0$, in the presence of dynamic model and parametric actuator uncertainty which presented via numerical simulations in Section 4.4.

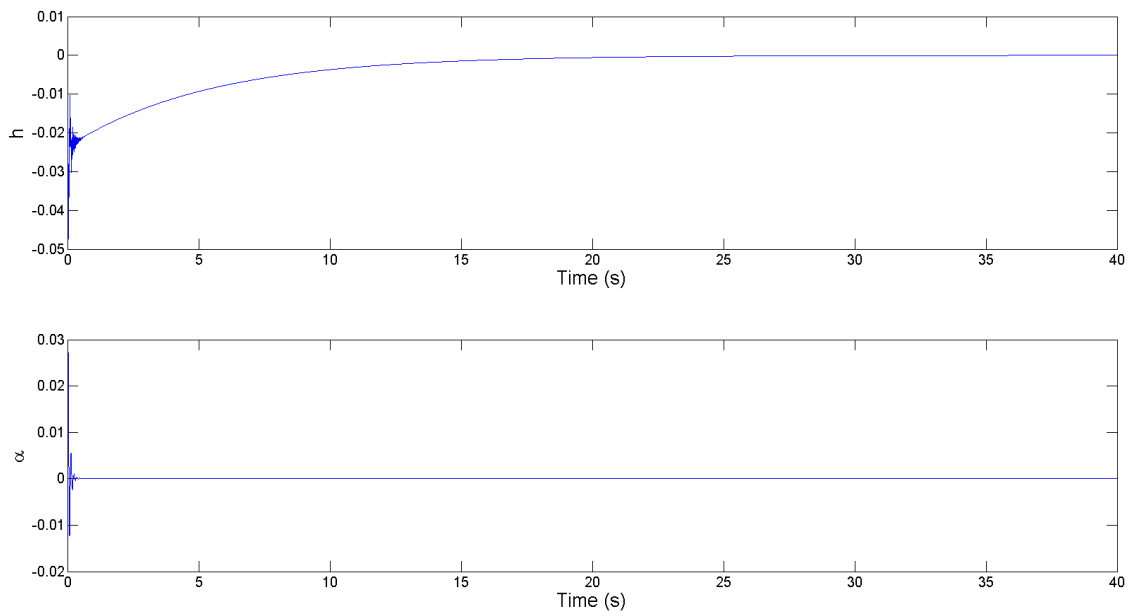Figure 4.1: Convergence of the control input behavior, u, tracking error for plunging, h in $[m]$, and pitching, α in $[rad]$.
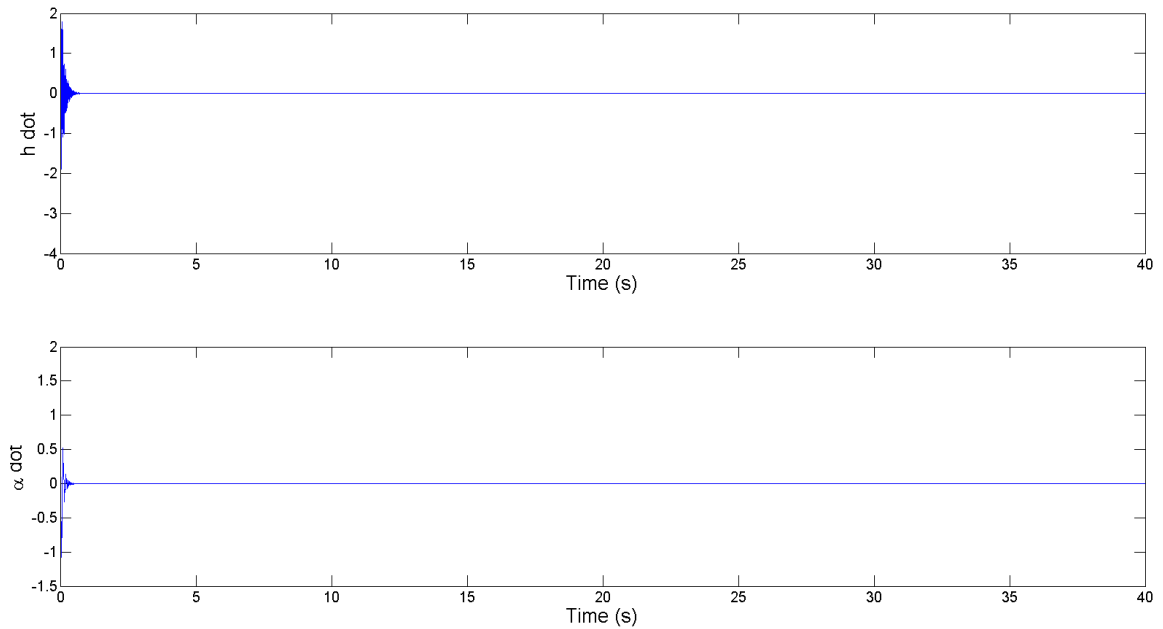
Figure 4.2: Convergence of the derivative of the tracking error for plunging, $\dot{h}$, and pitching, $\dot{\alpha}$.
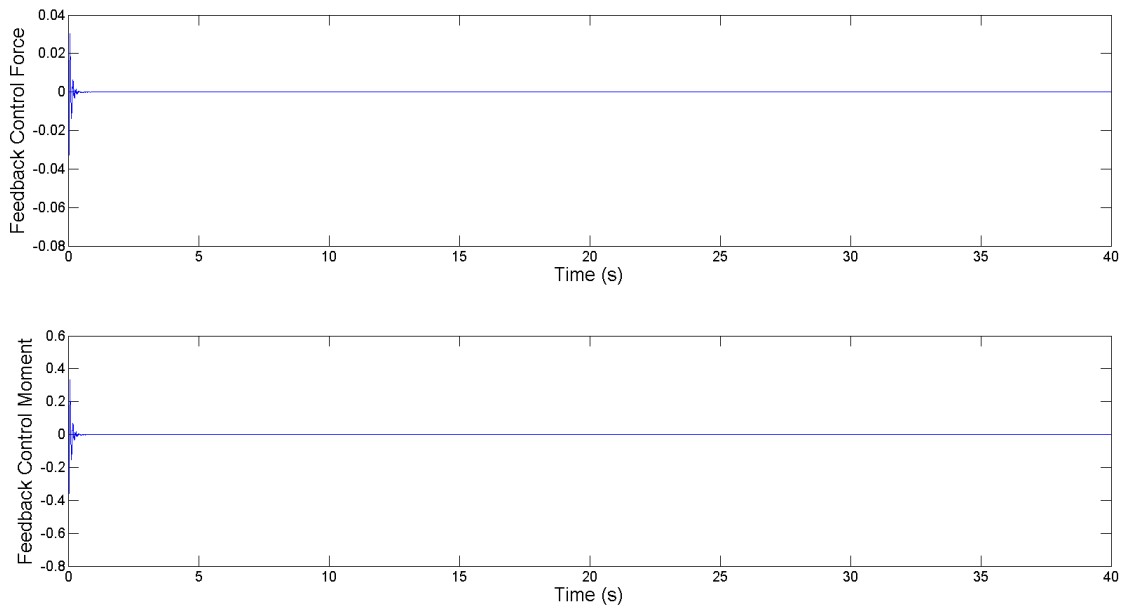
Figure 4.3: Feedback control force and moment.

Chapter 5

LCO supression with sliding mode control

5.1   Introduction

Control design for underactuated systems presents significant challenges. While backstepping-based approaches can be utilized for underactuated system in a cascade or normal form (Oland et al., 2013; Yoshimura et al., 2013; Gao et al., 2012), further challenges exist for systems in a parallel underactuated form, where backstepping techniques cannot be applied. There remains a need for computationally minimal robust nonlinear control methods, which can achieve asymptotic regulation for such "dual parallel systems", where a single scalar control input simultaneously affects two states. In this chapter, a nonlinear robust controller is demonstrated to suppress both pitching and plunging LCO in an UAV wing using a single scalar control input. In addition, the proposed control design compensates for the inherent SJA nonlinear-

ity using a robust inverse controller structure (Mackunis et al., 2013). Specifically, asymptotic LCO regulation is achieved using a sliding mode control strategy with a periodic switching law. A detailed model of the UAV dynamics is utilized along with a rigorous analysis to prove asymptotic regulation of the plunging displacement, and numerical simulation results are provided to demonstrate asymptotic suppression of both pitching and plunging displacements.

5.2 Dynamic Model

The equation describing LCO can be expressed as (Elhami & Narab Fatehi, 2012) (see Fig. 5.1 and 5.2)

$$M_s\ddot{p} + C_s\dot{p} + F(p)p = \begin{bmatrix} -\text{Lift} \\ \text{Moment} \end{bmatrix} \tag{5.1}$$

where the coefficients M_s, $C_s \in \mathbb{R}^{2\times2}$ denote the structural mass and damping matrices, $F(p) \in \mathbb{R}^{2\times2}$ is a nonlinear stiffness matrix, and $p(t) \in \mathbb{R}^2$ denotes the state vector.
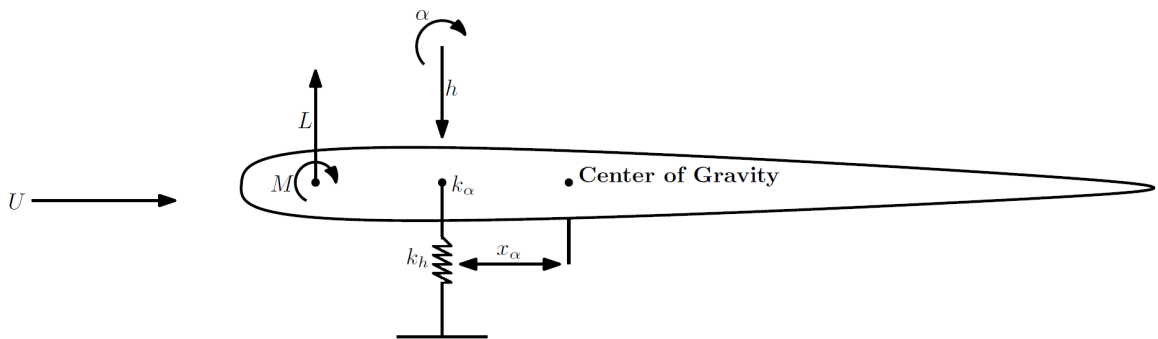
Figure 5.1: Pitching, α, and plunging, h, in an airfoil.
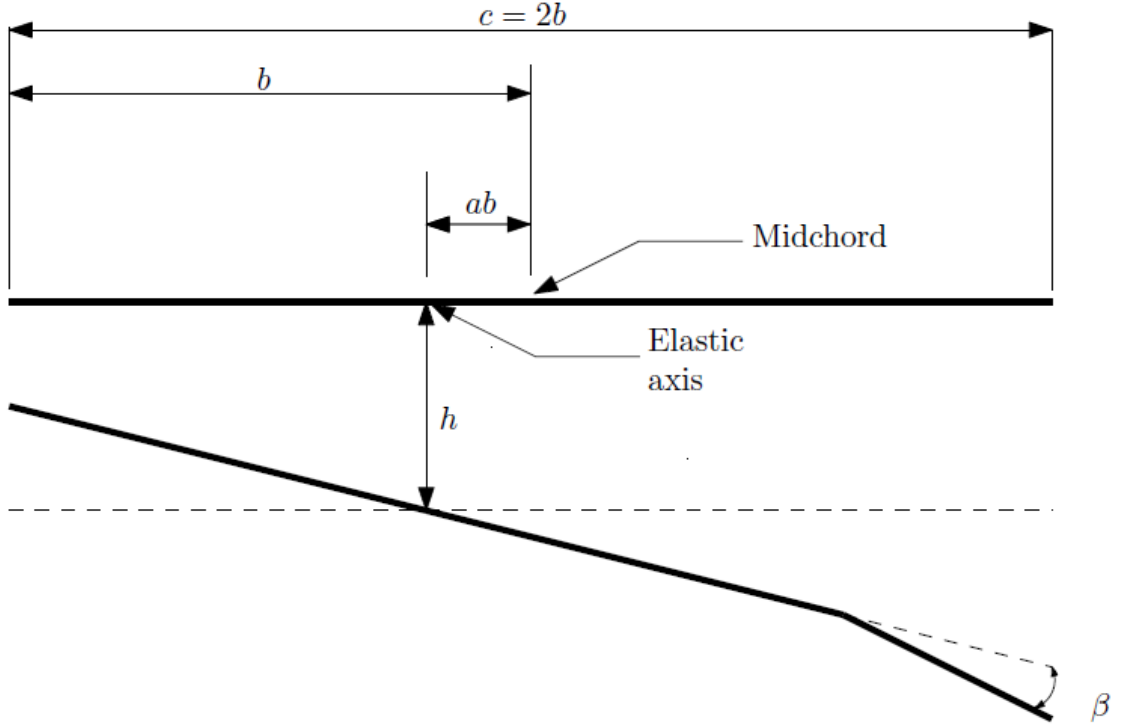
Figure 5.2: Diagram of the wing section.

In (5.1), $p(t)$ is defined as

$$p = \begin{bmatrix} h \\ \alpha \end{bmatrix} \qquad (5.2)$$

where $h(t)$, $\alpha(t) \in \mathbb{R}$ denote the plunging $[meters]$ and pitching $[radians]$ displacements describing the LCO effects.

Also in (5.1), the structural linear mass matrix M_s is defined as (Elhami & Narab Fatehi, 2012)

$$M_s = \begin{bmatrix} m & mx_\alpha b \\ mx_\alpha b & I_\alpha \end{bmatrix} \qquad (5.3)$$

where the parameters $x_\alpha \in \mathbb{R}$ denotes the nondimensional distance measured from

the elastic axis to the center of mass, $b \in \mathbb{R}$ is the semi-chord of the wing $[m]$, m mass of the wing section $[kg]$, and I_α is the mass moment of inertia of the wing about the elastic axis $[kg \cdot m^2]$ (see Fig. 5.1 and 5.2) The structural linear damping matrix is described as

$$C_s = \begin{bmatrix} C_h & 0 \\ 0 & C_\alpha \end{bmatrix} \tag{5.4}$$

where the parameters C_h, $C_\alpha \in \mathbb{R}$ are the structural damping coefficient in plunge due to viscous damping $\left[\frac{kg}{s}\right]$, and structural damping coefficient in pitch due to viscous damping $\left[\frac{kg \cdot m^2}{s}\right]$, respectively. The nonlinear stiffness matrix utilized in this study is

$$F(p) = \begin{bmatrix} K_h & 0 \\ 0 & K_\alpha \end{bmatrix} \tag{5.5}$$

where $K_h \in \mathbb{R}$ is the structural spring constant in plunge $\left[\frac{N}{m}\right]$ and $K_\alpha \in \mathbb{R}$ in $\left[\frac{N \cdot m}{rad}\right]$ is the torsion stiffness coefficient described as a polynomial as

$$K_\alpha = 2.82 \left(1 - 22.1\alpha + 1315.5\alpha^2 - 8580\alpha^3 + 17289.7\alpha^4\right) \tag{5.6}$$

Also in (5.1), the force L and moment M are described explicitly as

$$\begin{aligned} L &= \rho U^2 s_p b c_{l_\alpha} \left[\alpha + \frac{\dot{h}}{b} + \left(\frac{1}{2} - a\right) b \frac{\dot{\alpha}}{U}\right] \\ &+ \rho U^2 s_p b c_{l_\beta} \beta \end{aligned} \tag{5.7}$$

$$\begin{aligned} M &= \rho U^2 s_p b^2 c_{m_\alpha} \left[\alpha + \frac{\dot{h}}{b} + \left(\frac{1}{2} - a\right) b \frac{\dot{\alpha}}{U}\right] \\ &+ \rho U^2 s_p b^2 c_{m_\beta} \beta \end{aligned} \tag{5.8}$$

where $U \in \mathbb{R}$ is the velocity $\left[\frac{m}{s}\right]$, ρ is the density of air $\left[\frac{kg}{m^3}\right]$, s_p is the wing span $[m]$, c_{l_α} is lift coefficient per angle of attack, c_{m_α} is the moment coefficient per control surface deflection, c_{l_β} is the lift coefficient per control surface deflection, c_{m_β} is the moment coefficient per control surface deflection, and a is the non-dimensional distance from the mid-chord to elastic axis. The term β is the surface deflection angle of the wing. By rearranging (5.1), the dynamics equations are transformed into a state space in the form of

$$\dot{x} = A(x)x + B\beta \tag{5.9}$$

where $\beta \in \mathbb{R}$ denotes the surface deflection angle, $x(t) \in \mathbb{R}^4$ is the state vector, $A(x) \in \mathbb{R}^{4 \times 4}$ is the state matrix, and $B \in \mathbb{R}^{4 \times 1}$ is the control gain. Expanding (5.9), the state space equation can be expressed as

$$\dot{x} = \begin{bmatrix} 0 & 0 & 1 & 0 \\ 0 & 0 & 0 & 1 \\ a_1 & a_2 & a_3 & a_4 \\ c_1 & c_2 & c_3 & c_4 \end{bmatrix} x + F(x_2) + \begin{bmatrix} 0 \\ 0 \\ b_1 \\ b_2 \end{bmatrix} u \tag{5.10}$$

where $F(x_2) \in R^{4 \times 1}$ contains the nonlinear stiffness terms, which are dependent on the pitching displacement, α. In (5.10), $u(t) \in \mathbb{R}$ denotes the virtual surface deflection resulting from the SJA (see β in (5.9)). The explicit definition of the matrix A can

be found in Appendix A. The nonlinear stiffness $F(x_2)$ is explicitly defined

$$F(x_2) = \begin{bmatrix} 0 \\ 0 \\ \dfrac{-K_\alpha}{m\left(x_a b - \dfrac{I_\alpha}{m x_a b}\right)} \\ \dfrac{\dfrac{1}{x_a b}K_\alpha}{m\left(x_a b - \dfrac{I_\alpha}{m x_a b}\right)} \end{bmatrix} \alpha \tag{5.11}$$

Also in (5.10), the b_1, b_2 variables are given by

$$b_1 = \frac{\rho v^2 b^2 c_{m\beta} s_p + \dfrac{I_\alpha}{m x_a b}\rho v^2 b c_{l\beta} s_p}{m\left(x_a b - \dfrac{I_\alpha}{m x_a b}\right)} \tag{5.12}$$

$$b_2 = \frac{-\rho v^2 b c_{l\beta} s_p - \dfrac{1}{x_a b}\rho v^2 b^2 c_{m\beta} s_p}{m\left(x_a b - \dfrac{I_\alpha}{m x_a b}\right)} \tag{5.13}$$

Consequently, by making the following definitions, $x_1 = h$, $x_2 = \alpha$, $x_3 = \dot{h}$, and $x_4 = \dot{\alpha}$; and defining $\dot{x}_1 = x_3$, $\dot{x}_2 = x_4$, $\dot{x}_3 = \ddot{h}$, and $\dot{x}_4 = \ddot{\alpha}$, the state vector and its derivative can be expressed as

$$x \triangleq \begin{bmatrix} x_1 & x_2 & x_3 & x_4 \end{bmatrix}^T \tag{5.14}$$

$$\dot{x} \triangleq \begin{bmatrix} \dot{x}_1 & \dot{x}_2 & \dot{x}_3 & \dot{x}_4 \end{bmatrix}^T \tag{5.15}$$

5.3 SJA dynamics

Based on empirical data, the dynamics of an SJA are modeled as (Deb et al., 2005a, 2006, 2007, 2008)

$$u = \theta_2^* - \frac{\theta_1^*}{v} \tag{5.16}$$

where $u(t) \in \mathbb{R}$ denotes the virtual airfoil surface deflection (i.e., the control force), $v(t) = A_{ppi}^2(t) \in \mathbb{R}$ denotes the peak-to-peak voltage in $[Volts]$, and θ_1^*, $\theta_2^* \in \mathbb{R}$ are uncertain physical parameters in $[Volt - deg]$ and $[deg]$, respectively.

To compensate for the control input nonlinearity and input parametric uncertainty in (5.16), a robust inverse $v(t)$ based on (Mackunis et al., 2013) is utilized, which incorporates constant, "best-guess" feedforward estimates of the uncertain parameters, θ_1^*, θ_2^*. This robust inverse can be expressed as

$$v(t) = \frac{\hat{\theta}_1}{\hat{\theta}_2 - u_d} \tag{5.17}$$

where $\hat{\theta}_1$, $\hat{\theta}_2 \in \mathbb{R}$ are the constant feedfoward estimates of θ_1^*, θ_2^*, and $u_d(t) \in \mathbb{R}$ is a subsequently defined auxiliary control signal.

5.4 Control Development

The objective is to design the scalar control signal u_d to regulate the plunging and pitching dynamics (i.e., $h(t)$ and $\alpha(t)$) to zero. By utilizing the definition of u_d

provided from (Drakunov, 1994) as

$$u_d = M_0 \tanh \left\{ \sin \left[\frac{\pi}{\epsilon} \left(s(t) + \lambda \int_0^t \tanh(s(\tau))d\tau \right) \right] \right\} \qquad (5.18)$$

The sliding surface described below is based on the dynamic equation in (5.15).

$$s(x) = -\frac{K_\alpha}{d}x_2 + k_1 x_1 + k_2 x_3 + \sum_{i=1}^{4} a_i x_i \quad i = 1, \ldots, 4 \qquad (5.19)$$

where a_i are the coefficients that are obtained from (5.10) and d is defined as

$$d = m \left(x_a b - \frac{I_\alpha}{m x_a b} \right) \qquad (5.20)$$

It can be shown from (5.19), that the function $B(x, t)$ for all $t > 0$ satisfies the controllability condition

$$G(x)B^T(x, t) \neq 0 \qquad (5.21)$$

where $G(x) = \frac{\partial s(x)}{\partial x}$ (Drakunov, 1994).

5.5 Stability Analysis

Theorem 3. *The robust control law in (5.18) ensures asymptotic convergence to the sliding manifold $s(x) = 0$.*

Proof. Proof of Theorem 3 can be found in (Drakunov, 1994). □

Theorem 4. *It can be shown that $s(x) \to 0 \Rightarrow \dot{x}_3 = -k_1 x_3 - k_2 x_1$. This results in*

$\Rightarrow x_1 = h(t) \to 0$, *and* $x_3 = \dot{h}(t) \to 0$; *and the simulation results show that* $h(t)$, $\alpha(t) \to 0$. *The simulation results further show that asymptotic regulation of both the pitching and plunging displacements is achieved using the proposed sliding mode control law.*

5.6 Results

A numerical simulation was created to demonstrate the performance of the control law developed in (5.18). The simulation is based on the dynamic model given in (5.1). The dynamic parameters utilized in the simulation are summarized in Table 5.3 and were obtained from (Elhami & Narab Fatehi, 2012).

The control gains k_s, ϵ, M_0, and λ were manually selected and described in Table 5.1. The actual θ_1^*, and θ_2^* and estimates $\hat{\theta}_1$, and $\hat{\theta}_2$ are described in Table 5.2.

Table 5.1: Manually selected gains for robust control

$k_s = 9.0$	$\epsilon = 100$
$M_0 = 1.0$	$\lambda = 17.0$

Table 5.2: Feedforward estimates

$\theta_1^* = 32.9 Volt - deg$	$\hat{\theta}_1 = 32.9 Volt - deg$
$\theta_2^* = 14.7 deg$	$\hat{\theta}_2 = 14.7 deg$

The initial condition of the state vector, x, is given by

$$x = \begin{bmatrix} 0.02 & 0.2 & 0 & 0 \end{bmatrix}^T \tag{5.22}$$

Fig. 5.4 shows the time evolution of $h(t)$, which demonstrates the rapid convergence of the system plunge to zero. Furthermore, Fig. 5.4 also shows that the pitching displacement $\alpha(t)$ also converges to zero quickly, as well as the control effort $(u(t))$ used during closed-loop controller operation. In, Fig. 5.4, shows the convergence of the derivative for plunging, $\dot{h}$, and pitching, $\dot{\alpha}$. Again, the commanded control input remains within reasonable limits throughout the duration of the simulation.
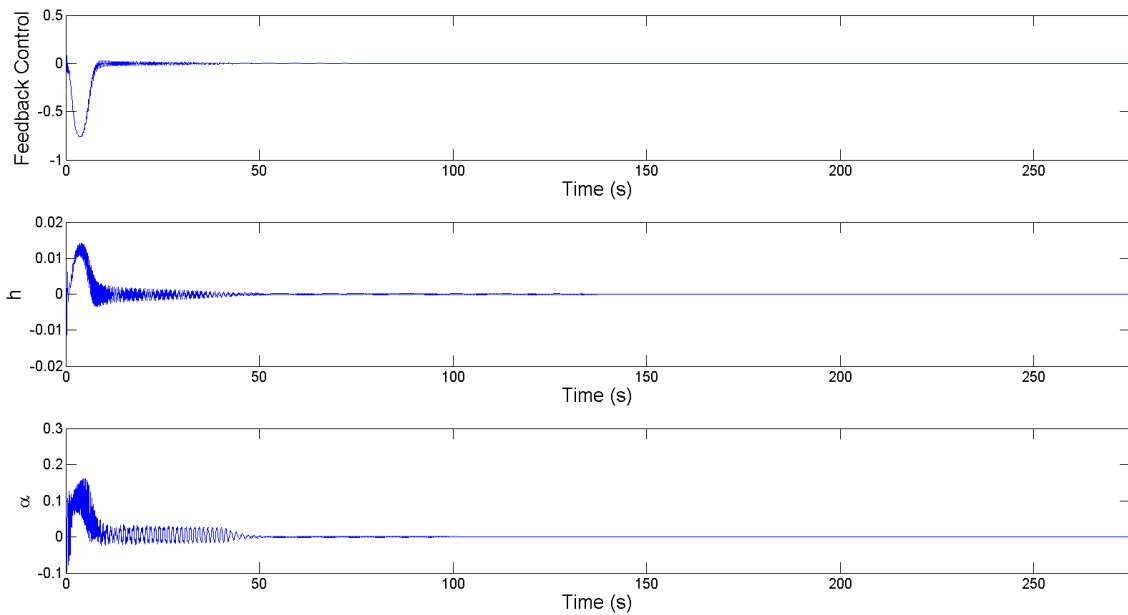
Figure 5.3: Convergence of the control input behavior, u, tracking error for plunging, h in $[m]$, and pitching, α in $[rad]$.
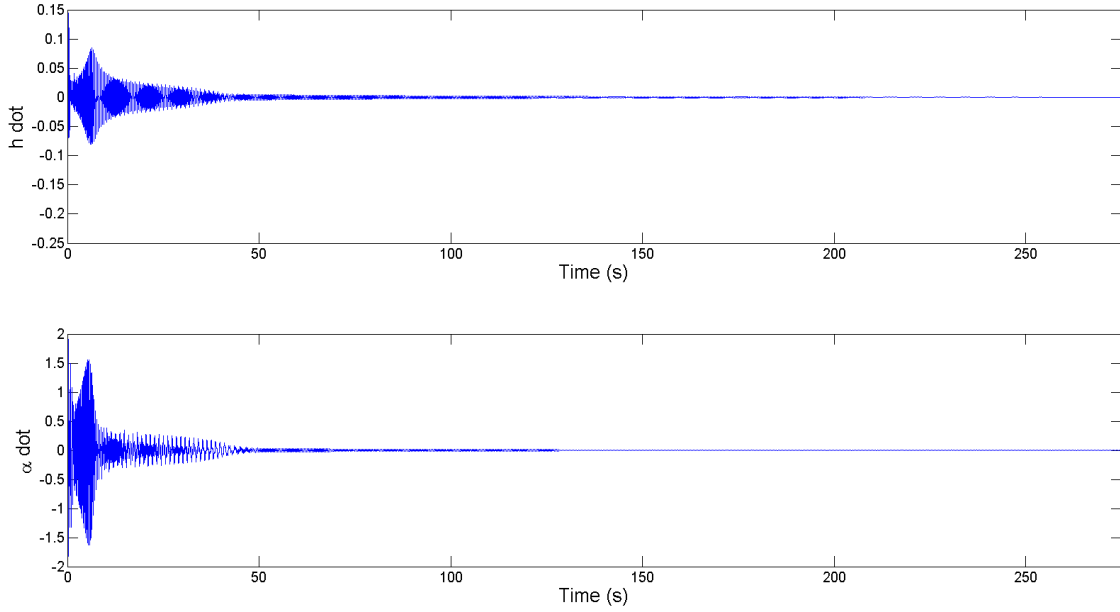
Figure 5.4: Convergence of the derivative of the tracking error for plunging, $\dot{h}$, and pitching, $\dot{\alpha}$.

Table 5.3: Constant parameters

$\rho = 1.225\frac{kg}{m^3}$	$a = -0.6$	$c_{m_\alpha} = -0.635$
$m = 12.387kg$	$b = 0.125m$	$v = 13\frac{m}{s}$
$C_\alpha = 0.036\frac{kg \cdot m^2}{s}$	$c_{l_\beta} = 3.358$	$s_p = 0.6m$
$I_\alpha = 0.065kg \cdot m$	$C_h = 27.43\frac{kg}{s}$	$c_{l_\alpha} = 6.28$
$K_h = 2844.4\frac{N}{m}$	$c_{m_\beta} = -0.635$	$x_a = 0.2847$

5.7   Conclusion

In this chapter, a nonlinear sliding mode control law for SJA-based LCO suppression in UAV wings is presented. The sliding mode control law in Section 5.4 achieves global asymptotic regulation of the pitching and plunging displacements to zero, using a single scalar control input (i.e., the single-input two-output control problem).

Moreover, since the dynamic model is in a parallel underactuated form, standard backstepping-based control techniques cannot be applied. This challenge is mitigated through innovative design of a sliding surface and application of a sliding mode control law incorporating a periodic switching function. Numerical simulation results are presented to demonstrate convergence of both pitching and plunging displacements to zero.

Chapter 6

Conclusions

This thesis, it presented three nonlinear SJA-based control methods to suppress the LCO in a UAV wing. The first method was utilized an adaptive control law, which achieves global asymptotic regulation of the plunging, $h \to 0$, while simultaneously regulating the pitching, $\alpha \to 0$. The second method is a simplistic robust (with a single feedback loop) nonlinear controller, which achieves asymptotic regulation of the pitching and plunging displacements to zero, $(h, \alpha) \to 0$, in the presence of uncertainty and parametric actuator uncertainty. The third method addresses the nonlinear control of a dual parallel underactuated system, where standard backstepping-based techniques cannot be applied. Moreover, the proposed approach compensates for the inherent SJA nonlinearity to achieve asymptotic regulation of pitching and plunging displacements to zero, $(h, \alpha) \to 0$. Rigorous Lyapunov-based stability analyses are utilized to prove the theoretical results, and numerical simulation results are provided to demonstrate the performance of the proposed control laws.

Appendix A

Coefficients

These are the coefficients of the A matrix discussed in Chapter 5.

$$a_1 = \frac{\dfrac{I_\alpha}{mx_ab}K_h}{m\left(x_ab - \dfrac{I_\alpha}{mx_ab}\right)} \tag{A.1}$$

$$a_2 = \frac{\rho v^2 b^2 c_{m\alpha} s_p + \dfrac{I_\alpha}{mx_ab}\rho v^2 b c_{l\alpha} s_p}{m\left(x_ab - \dfrac{I_\alpha}{mx_ab}\right)} \tag{A.2}$$

$$a_3 = \frac{\rho v b^2 c_{m\alpha} s_p + \dfrac{I_\alpha}{mx_ab}C_h + \dfrac{I_\alpha}{mx_ab}\rho v b s_p c_{l\alpha}}{m\left(x_ab - \dfrac{I_\alpha}{mx_ab}\right)} \tag{A.3}$$

$$a_4 = \frac{-C_\alpha + \rho v b^3 c_{m\alpha} s_p \left(\frac{1}{2} - a\right) + \dfrac{I_\alpha}{mx_ab}\rho v b^2 c_{l\alpha} s_p \left(\frac{1}{2} - a\right)}{m\left(x_ab - \dfrac{I_\alpha}{mx_ab}\right)} \tag{A.4}$$

$$c_1 = \frac{-K_h}{m\left(x_a b - \dfrac{I_\alpha}{m x_a b}\right)} \tag{A.5}$$

$$c_2 = \frac{-\rho v^2 b c_{l\alpha} s_p + \dfrac{1}{x_a b}\rho v^2 b^2 s_p c_{m\alpha}}{m\left(x_a b - \dfrac{I_\alpha}{m x_a b}\right)} \tag{A.6}$$

$$c_3 = \frac{-C_h - \rho v b c_{l\alpha} s_p + \dfrac{1}{x_a b}\rho v b^2 s_p c_{m\alpha}}{m\left(x_a b - \dfrac{I_\alpha}{m x_a b}\right)} \tag{A.7}$$

$$c_4 = \frac{-\rho v b^2 c_{l\alpha} s_p \left(\frac{1}{2} - a\right) + \dfrac{1}{x_a b}\left(C_\alpha - \rho v b^3 c_{m\alpha} s_p \left(\frac{1}{2} - a\right)\right)}{m\left(x_a b - \dfrac{I_\alpha}{m x_a b}\right)} \tag{A.8}$$

Appendix B

Simulink Models

These are the block diagrams that represents the work done in Chapter 3.
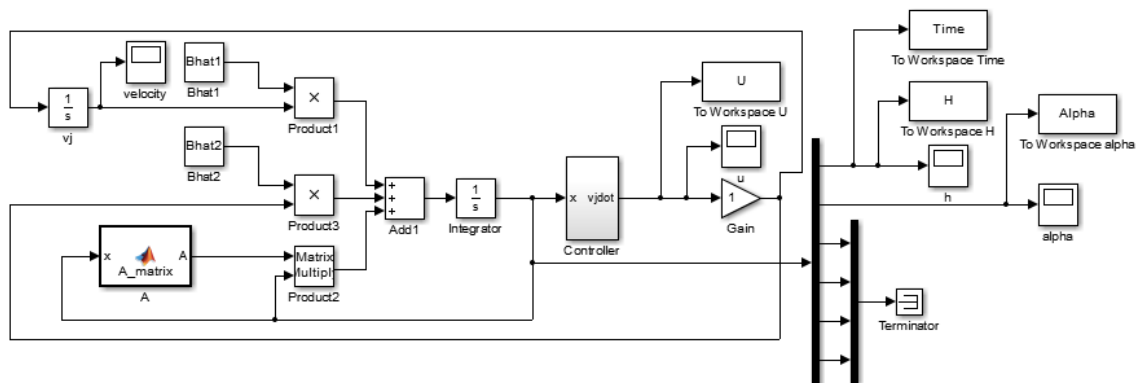
Figure B.1: An adaptive control system
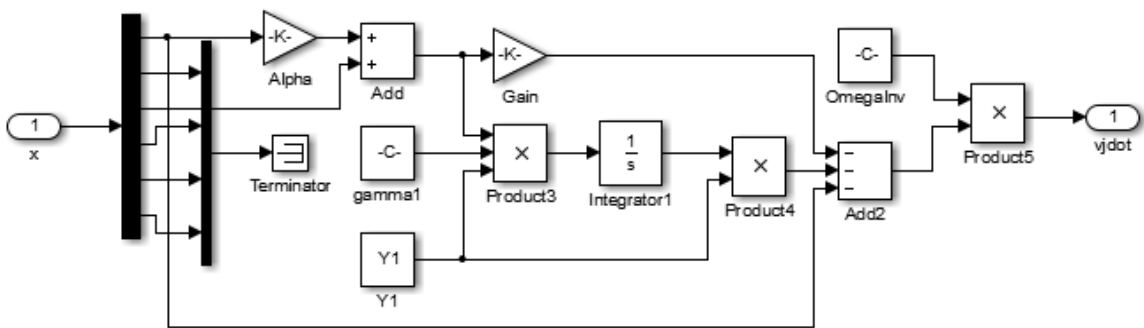
Figure B.2: An adaptive controller

Appendix C

MatLab Codes

The following two $m-$files are used for the work in Chapter 3.

`Constants.m`

```matlab
1  %Values
2  rho = 1.225; % kg/m^3
3  a = -0.24;
4  b = 0.11; % m
5  ma = 2.55; % kg
6  Sa = 10.4e-3; % kg*m
7  Ia = 2.51e-3; % kg*m^2
8  v = 18; % m/s
9
10 %Synthetic Jet locations
11 theta1 = 1.6;
12 theta2 = 1.7;
13
```

```matlab
% Distributed forces
I1 = (theta2 - ...
    theta1)*((sin(theta1)*atan(theta1/2)+sin(theta2)*atan(theta2/2))/2);
I2 = 1/2*(theta2 - theta1 + 1/2*sin(2*theta1)-1/2*sin(2*theta2));
I3 = 1/3*(sin(theta2)^3 - sin(theta1)^3);

% M matrix
M = ma + pi*rho*b^2;
S = Sa - pi*rho*b^3*a;
I = Ia + pi*rho*b^4*(1/8 - a^2);
Mass = [M S; S I];

% B1 matrix
B1 = zeros(2,1);
B1(1,1) = -v*rho*b*I1;
Y1 = B1(1,1);
B1(2,1) = b^2*v*rho*I2 + a*v*rho*b^2*I1;
B1hat = Mass^(-1)*B1;
Bhat1 = zeros(6,1);
Bhat1(3:4) = B1hat;

% B2 matrix
B2 = zeros(2,1);
B2(1,1) = -v*rho*I2;
Y2 = B2(1,1);
B2(2,1) = -1/2*rho*b^3*I3+a*rho*b^3*I2;
B2hat = Mass^(-1)*B2;
Bhat2 = zeros(6,1);
Bhat2(3:4) = B2hat;
```

```
42
43   % Omega
44   Omega = B2(1,1);
45   OmegaInv = pinv(Omega);
46
47   % Gain
48   alpha = 2.5;
49   ks = 1;
50   gamma1 = 1;
```

A.m

```
1   function A = A_matrix
2   %#codegen
3
4   % Values
5   kh = 1;
6   ka = 1;
7   zeta_h = 1;
8   zeta_a = 1;
9   rho = 1;
10  U = 1;
11  a = 1;
12  b = 1;
13  a1 = 1;
14  b1 = 1;
```

```matlab
15  a2 = 1;

16  b2 = 1;

17  ma = 1;

18  Sa = 1;

19  Ia = 1;

20  phi_zero = 1;

21

22  % M matrix

23  M = ma + pi*rho*b^2;

24  S = Sa - pi*rho*b^3*a;

25  I = Ia + pi*rho*b^4*(1/8 - a^2);

26

27  % Making the A matrix

28  A = zeros(6);

29  A(1,3) = 1;

30  A(2,4) = 1;

31  A(3,1) = -kh/M;

32  A(3,2) = -2*pi*rho*U^2*b*phi_zero/S;

33  A(3,3) = -(2*zeta_h*sqrt(kh*m)+2*pi*rho*U*b*phi_zero)/M;

34  A(3,4) = -(pi*rho*U*b^2 - 2*pi*rho*U*b^2*phi_zero*(1/2-a))/S;

35  A(3,5) = 2*pi*a1*b1*U/M;

36  A(3,6) = 2*pi*rho*a2*b2*U/S;

37  A(4,2) = (2*pi*rho*U^2*b^2*phi_zero*(1/2+a)-(ka+ka3*x(2)))/I;

38  A(4,3) = 2*pi*rho*U*b^2*phi_zero*(1/2+a)/S;

39  A(4,4) = ...
        -1/I*(2*zeta_a*sqrt(ka*Ia)+pi*rho*U*b^3*(1/2-a)-2*pi*rho*U*b^3*...

40          phi_zero*(1/2+a)*(1/2-a));

41  A(4,5) = -2*pi*rho*U*b^2*(1/2+a)*a1*b1/S;

42  A(4,6) = -2*pi*rho*U*b^2*(1/2+a)*a2*b2/I;
```

```matlab
43  A(5,2) = -U^2/b;

44  A(5,3) = -U/b;

45  A(5,4) = -U*(1/2-a);

46  A(5,5) = -U*b1/b;

47  A(6,2) = -U^2/b;

48  A(6,3) = -U/b;

49  A(6,4) = -U*(1/2-a);

50  A(6,6) = -U*b2/b;
```

The following $m-$file is used for the work in Chapter 4.

`RISE_code.m`

```matlab
1   clear

2   clc

3

4   %% Initial Conditions

5   T = 30;

6   dt = 0.001;

7   t = 0:dt:T;

8   N = length(t);

9   int = 0;

10

11  % Creating of the main vectors

12  x = zeros(6,N);

13  u = zeros(2,N);
```

```matlab
14  A = zeros(6);

15  B = zeros(2);

16  Bu_1 = zeros(2,N);

17  Bu = zeros(6,N);

18

19  % % X initial

20  x(:,1) = [0; 0; 1; 2; 0; 0];

21

22  % Control Gains

23  beta = [0.001 0; 0 25];

24  k_s = [0.00001 0; 0 0.11];

25  alpha_1 = [1 0; 0 35];

26  alpha_2 = [1 0; 0 35];

27

28  % B Matrix

29  B(1,1) = 0.9;

30  B(1,2) = 0.1;

31  B(2,1) = -0.1;

32  B(2,2) = 1.1;

33

34  %% Wing section model parameters

35  kh = 4.5E2; % N/m

36  ka = 9.3; % N/m

37  ka3 = 55; % N/m

38  zeta_h = 5.5e-3; % N m/(1/s)/m

39  zeta_a = 1.8e-2; %N/(m/s)/m

40  rho = 1.225; % kg/m^3

41  U = 18.0; % m/s

42  a = -0.24;
```

```matlab
43  b = 0.11;  % m
44  a1 = 0.1650;
45  b1 = 0.3350;
46  a2 = 0.0455;
47  b2 =  0.3000;
48  ma = 2.55; % kg
49  Sa = 10.4e-3; % kg*m
50  Ia = 2.51e-3; % kg*m^2
51  phi_zero = 0.5;
52
53
54  % Mass matrix
55  M = ma + pi*rho*b^2;
56  S = Sa - pi*rho*b^3*a;
57  I = Ia + pi*rho*b^4*(1/8 - a^2);
58  Mass = [M S; S I];
59
60  %% Main loop
61  for i = 1:N-1
62  % Making the A matrix
63  A(1,3) = 1;
64  A(2,4) = 1;
65  A(3,1) = -kh/M;
66  A(3,2) = -2*pi*rho*U^2*b*phi_zero/S;
67  A(3,3) = -(2*zeta_h*sqrt(kh*ma)+2*pi*rho*U*b*phi_zero)/M;
68  A(3,4) = -(pi*rho*U*b^2 - 2*pi*rho*U*b^2*phi_zero*(1/2-a))/S;
69  A(3,5) = 2*pi*a1*b1*U/M;
70  A(3,6) = 2*pi*rho*a2*b2*U/S;
71  A(4,2) = (2*pi*rho*U^2*b^2*phi_zero*(1/2+a)-(ka+ka3*x(2)^2))/I;
```

```matlab
72  A(4,3) = 2*pi*rho*U*b^2*phi_zero*(1/2+a)/S;

73  A(4,4) = ...
        -1/I*(2*zeta_a*sqrt(ka*Ia)+pi*rho*U*b^3*(1/2-a)-2*pi*rho*U*b^3*...
74          phi_zero*(1/2+a)*(1/2-a));

75  A(4,5) = -2*pi*rho*U*b^2*(1/2+a)*a1*b1/S;

76  A(4,6) = -2*pi*rho*U*b^2*(1/2+a)*a2*b2/I;

77  A(5,2) = -U^2/b;

78  A(5,3) = -U/b;

79  A(5,4) = -U*(1/2-a);

80  A(5,5) = -U*b1/b;

81  A(6,2) = -U^2/b;

82  A(6,3) = -U/b;

83  A(6,4) = -U*(1/2-a);

84  A(6,6) = -U*b2/b;

85

86  %

87  e1 = [x(1,i); x(2,i)];

88  e2 = [x(3,i); x(4,i)];

89

90  % Controller

91  B_hat = eye(2);

92  Bu_1(:,i) = ...
        0.02*100*B*inv(B_hat)*(-beta*tanh(e2+alpha_1*e1)*dt-k_s*(e2+(alpha_1+alpha_2)*e1+

93  Bu(:,i) = [0; 0; Bu_1(:,i); 0; 0];

94

95  % Solving the state variable with Euler's method

96  x(:,i+1) = x(:,i) + dt*(A*x(:,i)+ Bu(:,i));

97  end

98
```

```matlab
 99  figure(1)
100  plot(t, Bu_1(:,:))
101  xlabel('Time')
102  ylabel('Feedback Control Force/Moment')
103  legend('Force','Moment')
104  xlim([0 T])
105
106  figure(2)
107  subplot(2,1,1);
108  plot(t, x(1,:))
109  xlabel('Time')
110  ylabel('h')
111  xlim([0 T])
112
113  subplot(2,1,2);
114  plot(t, x(2,:))
115  xlabel('Time')
116  ylabel('\alpha')
117  xlim([0 T])
118
119  figure(3)
120  subplot(2,1,1);
121  plot(t, x(3,:))
122  xlabel('Time')
123  ylabel('h dot')
124  xlim([0 T])
125
126  subplot(2,1,2);
127  plot(t, x(4,:))
```

```matlab
128  xlabel('Time')
129  ylabel('\alpha dot')
130  xlim([0 T])
```

The following $m-$file is used for the work in Chapter 5.

`SITO_Robust.m`

```matlab
1   clear
2   clc
3
4   %% Initial Conditions
5   T = 10;
6   dt = 0.001;
7   t = 0:dt:T;
8   N = length(t);
9   int = 0;
10
11  % Creating of the main vectors
12  x = zeros(4,N);
13  u = zeros(1,N);
14  A = zeros(4);
15  F = zeros(4,1);
16  B = zeros(4,1);
17  theta_hat = zeros(2,6);
18
```

```matlab
19  % Initial condition of x
20  x(:,1) = [0.02;0.2;0;0];
21
22  %% Wing section model parameters
23  b = 0.125; % Semi chord [m]
24  C_a = 0.036; % Structural damping coefficient in pitch [kg*m^2/s]
25  c_lb = 3.358; % Lift coefficients per control surface deflection
26  m = 12.387; % Mass [kg]
27  s_p = 0.6; % Wing span [m]
28  K_h = 2844.4; % Structural spring constant in plunge [N/m]
29  rho = 1.225; % Density of air [kg/m^3]
30  I_a = 0.065; % Mass moment of inertia of the wing about the elastic ...
        axis [kg*m^2]
31  C_h = 27.43; % Structural damping coefficient in plunge [kg/s]
32  c_la = 6.28; % Lift coefficient per angle of attack
33  a = -0.6; % Non-dimensional distance from the mid chord to the ...
        elastic axis
34  c_mb = -0.635; % Moment coefficient per control surface deflection
35  x_a = 0.2847; % Non-dimensional distance measured from the elastic ...
        axis to center of mass
36  c_ma = -0.635; % Moment coefficient per angle of attack
37  v = 13; % Velocity [m/s]
38
39  %% Main loop
40  for i = 1:N-1
41  % Torsion Stiffness Coefficient
42  K_a = 2.82*(1 - 22.1*x(2,i) + 1315.5*x(2,i)^2 - 8580*x(2,i)^3 + ...
        17289.7*x(2,i)^4);
43
```

```matlab
44   % D coefficients
45   d1 = I_a/(m*x_a*b);
46   d2 = 1/(x_a*b);
47   d = m*(x_a*b-d1);
48
49   % A matrix coefficients without nonlinear terms
50   a1 = d1*K_h/d;
51   a2 = (rho*v^2*b^2*c_ma*s_p+d1*rho*v^2*b*c_la*s_p)/d;
52   a3 = (rho*v*b^2*c_ma*s_p + d1*(C_h + rho*v*b*s_p*c_la))/d;
53   a4 = (-C_a + rho*v*b^3*c_ma*(1/2 - a)*s_p + ...
          d1*rho*v*b^2*c_la*s_p*(1/2 - a))/d;
54   c1 = -K_h/d;
55   c2 = (-rho*v^2*b*c_la*s_p + d2*(rho*v^2*b^2*s_p*c_ma))/d;
56   c3 = (-C_h - rho*v*b*c_la*s_p + d2*rho*v*b^2*s_p*c_ma)/2;
57   c4 = (-rho*v*b^2*c_la*s_p*(1/2 - a) + d2*(C_a - ...
          rho*v*b^3*c_ma*s_p*(1/2 - a)))/d;
58
59   % A Matrix population
60   A(1,3) = 1;
61   A(2,4) = 1;
62   A(3,1) = a1;
63   A(3,2) = a2;
64   A(3,3) = a3;
65   A(3,4) = a4;
66   A(4,1) = c1;
67   A(4,2) = c2;
68   A(4,3) = c3;
69   A(4,4) = c4;
70
```

```matlab
71  % Nonlinear part of the A matrix

72  k1 = -K_a/d;

73  k2 = d2*K_a/d;

74

75  % Nonlinear vector

76  F = [0; 0; k1; k2];

77

78  % B coefficients

79  b1 = (rho*v^2*b^2*c_mb*s_p + d1*rho*v^2*b*c_lb*s_p)/d;

80  b2 = (-rho*v^2*b*c_lb*s_p - d2*rho*v^2*b^2*s_p*c_mb)/d;

81

82  % B matrix

83  B(3,1) = b1*cos(x(2,i));

84  B(4,1) = b2*sin(x(2,i));

85

86  % Gains

87  epsilon = 100;

88  lamda = 17.0;

89  M_0 = 1;

90

91  % Sliding Surface

92  a_all = [a1 a2 a3 a4];

93  c_all = [c1 c2 c3 c4];

94  ks = 9;

95  s = -(K_a/d)*x(2,i) + ks*x(3,i) + a_all*x(:,i);

96

97  % Drakunov Controller

98  int = dt*(tanh(s)) + int;

99  u(:,i) = M_0*tanh(sin(pi/epsilon*(s + lamda*int)));
```

```matlab
100
101  % Solving the state variable with Euler's method
102  x(:,i+1) = x(:,i) + dt*(A*x(:,i)+ F*x(2,i) + B*u(:,i));
103  end
104
105  %% Output
106
107  figure(1)
108  subplot(3,1,1);
109  plot(t, u(:,:))
110  xlabel('Time')
111  ylabel('Feedback Control')
112  xlim([0 T])
113
114  subplot(3,1,2);
115  plot(t, x(1,:))
116  xlabel('Time')
117  ylabel('h')
118  xlim([0 T])
119
120  subplot(3,1,3);
121  plot(t, x(2,:))
122  xlabel('Time')
123  ylabel('\alpha')
124  xlim([0 T])
125
126  figure(2)
127  subplot(2,1,1);
128  plot(t, x(3,:))
```

```matlab
129  xlabel('Time')

130  ylabel('h dot')

131  xlim([0 T])

132

133  subplot(2,1,2);

134  plot(t, x(4,:))

135  xlabel('Time')

136  ylabel('\alpha dot')

137  xlim([0 T])
```

References

Beran, P., Pettit, C., & Millman, D. (2006). Uncertainty quantification of limit-cycle oscillations. *Journal of Computational Physic*, *217*, 191-231.

Deb, D., Burkholder, J., & Smith, D. (2006). Adaptive synthetic jet actuator compensation for a nonlinear tailless aircraft model at low angles of attack. In *2006 american control conference* (p. 6). Minneapolis, MN: IEEE.

Deb, D., Tao, G., Burkholder, J. O., & Smith, D. R. (2005a). An Adaptive Inverse Control Scheme for A Synthetic Jet Actuator Model. In *American control conference* (Vol. 82071, pp. 2646–2651). Portland, OR: IEEE.

Deb, D., Tao, G., Burkholder, J. O., & Smith, D. R. (2005b, Sept. 26-29). An adaptive inverse control scheme for synthetic jet actuator arrays. In *Infotech@aerospace.*

Deb, D., Tao, G., Burkholder, J. O., & Smith, D. R. (2007, March). Adaptive Compensation Control of Synthetic Jet Actuator Arrays for Airfoil Virtual Shaping. *Journal of Aircraft*, *44*(2), 616–626.

Deb, D., Tao, G., Burkholder, J. O., & Smith, D. R. (2008). Adaptive Synthetic Jet Actuator Compensation for A Nonlinear Aircraft Model at Low Angles of Attack. *IEEE Transactions on Control Systems Technology*, *16*(5), 983–995.

Dixon, W. (2007). Adaptive regulation of amplitude limited robot manipulators with

uncertain kinematics and dynamics. *IEEE Transactions on Automatic Control*, *52*(3), 488–493.

Drakunov, S. (1994). Sliding mode control with multiple equilibrium manifolds. *ASME Dynamic Systems and Control*, *1*, 101-108.

Elhami, M., & Narab Fatehi, M. (2012). Comparison of SDRE and SMC Control Approaches for Flutter Suppression in a Nonlinear Wing Section. In *2012 american control conference* (p. 6148-6152). Montreal, Canada: AIAA.

Filippov, A. F. (1964). Differential equations with discontinuous right hand side. *American Math Society Transactions*, *42*(2), 191-231.

Frampton, K. D., & Clark, R. L. (2000). Experiments on control of limit cycle oscillations in a typical section. *Journal of Guidance, Control, and Dynamics*, *23*, 956–960.

Gao, B., Zhang, X., Yao, W., Guo, Y., Boa, Y., & Xie, J. (2012). Dynamics and motion control of an underactuated two-wheeled mobile robot. In *2012 ieee international conference on cyber technology in automation, control, and intelligent systems* (p. 179-184). Bangkok, Thailand.

Golubev, V. V., Dreyer, B. D., Hollenshade, T. M., & Visbal, M. R. (2009). High-Accuracy Viscous Simulation of Gust-Airfoil Nonlinear Aeroelastic Interaction. In *39th aiaa fluid dynamics conference* (p. 1-15). San Antonio, TX: AIAA Paper 2009-4200.

Jee, S. K., Lopez, O., Moser, R. D., Kutay, A. T., Muse, J. A., & Calise, A. J. (2009, June). Flow simulation of a controlled airfoil with synthetic jet actuators. In *AIAA conf. on computational fluid dynamics.* San Antonio TX.

Khalil, H. K. (2002). *Nonlinear Systems* (Vol. 3rd). Upper Saddle River, NJ: Prentice

Hall.

Landau, I., Lozano, R., M'Saad, M., & Karimi, A. (2011). *Adaptive control - algorithms, analysis and applications* (Vol. 2nd). New York City, NY: Springer.

Liu, Y., Ciuryla, M., Amitay, M., Kwan, C., Myatt, J. H., Zhang, X., ... Casey, J. P. (2006). Integrated flight control and flow control using synthetic jet arrays. In *Aiaa guidance, navigation, and control conference.* Keystone, CO.

Mackunis, W., Subramanian, S., Mehta, S., Ton, C., Curtis, J. W., & Reyhanoglu, M. (2013). Robust Nonlinear Aircraft Tracking Control Using Synthetic Jet Actuators. In *Ieee american control conference* (pp. 1–8). Eglin AFB, FL: IEEE.

MacKunis, W., Wilcox, Z., Kaiser, M. K., & Dixon, W. E. (2010). Global adaptive output feedback tracking control of an unmanned aerial vehicle. *IEEE Transactions on Control Systems Technology*, *18*(6), 1390–1397.

MacKunis, W., Wilcox, Z. D., Kaiser, M. K., & Dixon, W. E. (2009, Dec.). Global adaptive output feedback MRAC. In *Proceedings ieee conference on decision and control* (pp. 3483–3488). Shanghai, China.

Milanese, A., De Breuker, R., Marzocca, P., & Abdalla, M. (2008). Distributed Synthetic Jet Actuators for the Control of Nonlinear Aeroelastic Systems. In *19th international conference on adaptive structures and technologies* (pp. 1–12). Minneapolis, MN: ICAST.

Mondschein, S. T., Tao, G., & Burkholder, J. O. (2011, June-July). Adaptive actuator nonlinearity compensation and disturbance rejection with an aircraft application. In *American control conference* (pp. 2951–2956).

O'Donnell, K. S., Marzocca, P., & Milanese, A. (2007). Design of a Wind Tun-

nel Apparatus to assist Flow and Aeroelastic Control via Zero Net Mass Flow Actuators. In *Structures, structural dynamics, and materials conference* (pp. 1–12).

Oland, E., Schlanbush, R., & Kristiansen, R. (2013). Underactuated translational control of a rigid spacecraft. In *2013 ieee aerospace conference* (p. 1-7). Big Sky, Montana.

Platanitis, G., & Strganac, T. W. (2004). Control of a Nonlinear Wing Section Using Leading- and Trailing-Edge Surfaces. *Journal of Guidance, Control, and Dynamics*, *27*(1), 52–58.

Ramos Pedroza, N., MacKunis, W., Guenthoer, B., Golubev, V., & Curtis, J. (2014). Lyapunov-Based Adaptive Regulation of Limit Cycle Oscillations in Aircraft Wings Using Synthetic Jet Actuators. In *19th ifac world congress* (p. 6). Cape Town, South Africa.

Rubillo, C., Bollt, E., & Marzocca, P. (2005). Active Aeroelastic Control of Lifting Surfaces via Jet Reaction Limiter Control. In *Structures, structural dynamics, and materials conference* (pp. 18–21).

Satak, N., Hernandez, E. A. P., & Hurtado, J. E. (2012). Rate-free Control of Nonlinear Wing Section using Pitch and Plunge Measurements Only. In *Aiaa structures, structural dynamics and materials conference* (pp. 1–7). Honolulu, Hawaii: AIAA.

Singhal, C., Tao, G., & Burkholder, J. O. (2009). Neural network-based compensation of synthetic jet actuator nonlinearities for aircraft flight control. In *Aiaa guidance, navigation, and control conf.* Chicago, IL.

Stewart, J. (2012). *Calculus* (Vol. 7th). Independence, KY: Cengage Learning.

Strganac, T. W., K., J., & Thompson, D. E. (2000). Identification and control of limit cycle oscillations in aeroelastic systems. *Journal of Guidance, Control, and Dynamics*, *23*, 1127–1133.

Tao, G. (1996). *Adaptive control of systems with actuator and sensor nonlinearities.* John Wiley and Sons.

Tchieu, A. A., Kutay, A. T., Muse, J. A., Calise, A. J., & Leonard, A. (2008). Validation of a low-order model for closed-loop flow control enable flight. AIAA Paper 2008-3863.

Theodorsen, T. (1935). General Theory of Aerodynamic Instability and the Mechanism of Flutter. *NACA Technical Report*(496).

Utkin, V. I. (1992). *Sliding modes in control and optimization* (Vol. 116). Springer-Verlag Berlin.

Yoshimura, S., Watanabe, K., & Maeyama, S. (2013). Quasi-continuous exponential stabilization for the underactuated control of a fire truck robot by using an invariant manifold theory. In *2013 ieee international conference on mechatronics and automation* (p. 692-697). Takamatsu, Japan.